Architecting tomorrow

New 3GPP UE antenna and near-field blocking models for handheld devices

White paper

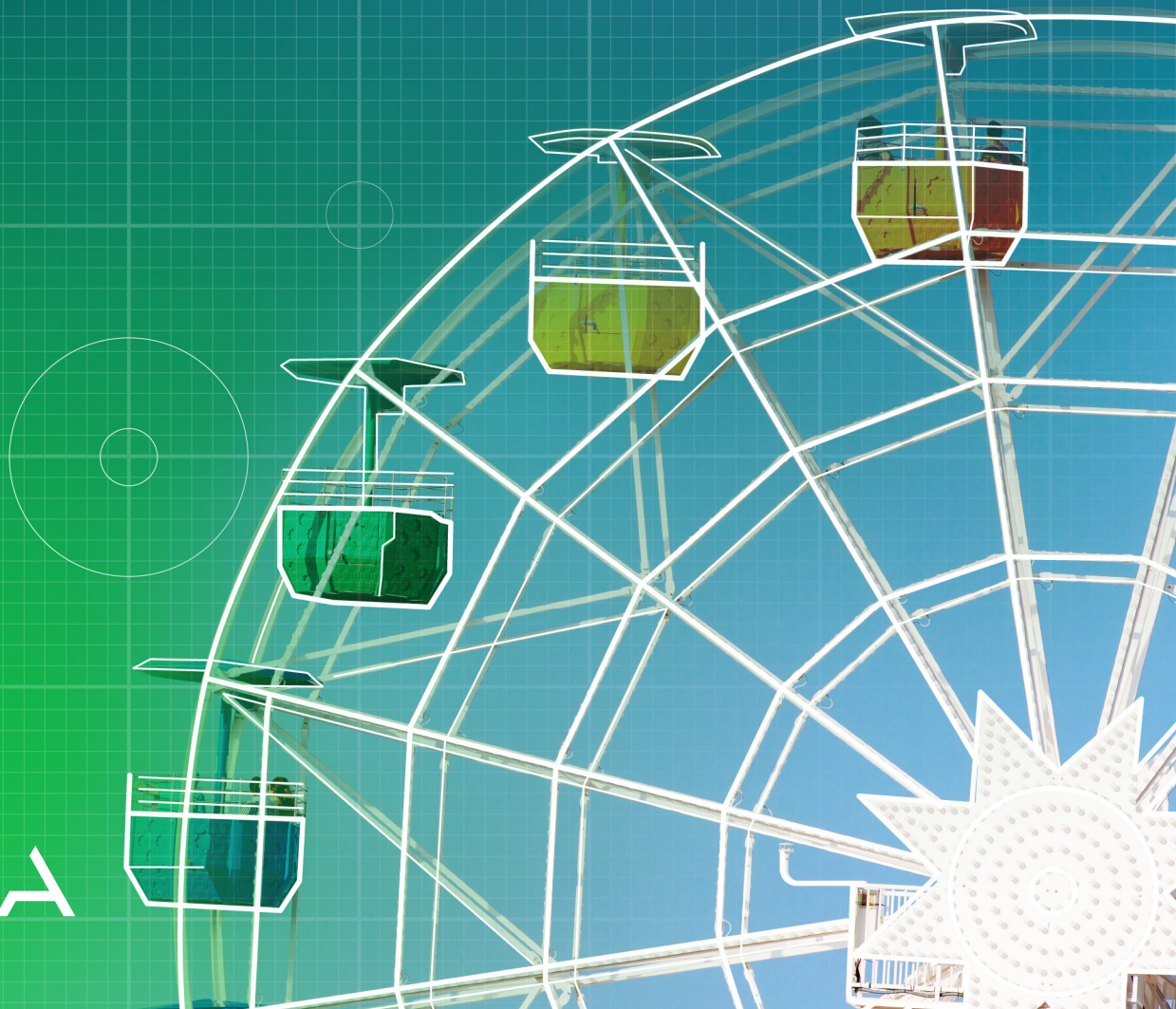

NOKIA

Contents

Executive summary

As we transition from 5G to 6G, the user equipment (UE) antenna model defined in 3GPP Rel-19 already anticipates the arrival of 6G by updating the older model from Rel-15. The Rel-19 model addresses the need for more accurate behavior in link- and system-level simulations for a closer alignment with real-life results and behavior. In this paper, we examine the new UE antenna model and its success at addressing these shortcomings. We examine a variety of simulations to gauge how closely they align with real-world conditions, including a Nokia proposal for a new UE antenna model that could be adopted by the existing framework already specified within 3GPP. Our goal in this work is to enable the 6G UE antenna model to more accurately assess device performance, leading to better design and optimization of mobile technologies and enhancing the overall user experience in diverse environments.

Introduction

The transition from one generation of mobile communication technology to the next is a pivotal moment for innovation and improvement. As we move from 5G to 6G, the user equipment (UE) antenna model within the 3rd Generation Partnership Project (3GPP) has already been redefined in Rel-19 (last release for 5G) as preparation for 6G. The motivation for this change is driven by the need to achieve more accurate behavior in link-level simulations (LLS) and system-level simulations (SLS), ensuring that the simulation results get a closer alignment with real-life results and behavior. The current 5G UE antenna model selected back in Rel-15, while functional, does not adequately capture the complexities of realistic characteristics for antennas implemented on handheld devices, leading to discrepancies between simulated and actual devices and inaccuracies in network performance evaluations. This gap becomes increasingly problematic as mobile technologies advance and user expectations rise. The transition to 6G presents an ideal opportunity to introduce a new UE antenna model that addresses these shortcomings. By aligning simulations more closely with real-world conditions, the new model will enable more accurate assessments of device performance, leading to better design and optimization of mobile technologies. This shift is not just about improving technical accuracy; it is about enhancing the overall user experience by ensuring that mobile devices perform as expected in diverse environments.

Rel-15 3GPP UE antenna model

The UE antenna model used for 5G (Rel-15) is the same UE antenna model that was defined in the early LTE days for Rel-8, in 2008, and was used as a reference model during the initial specification and later enhancements of 5G.

Rel-15 3GPP UE antenna pattern

3GPP Rel-15 UE antenna patterns are based on total gain of either an isotropic radiator or as a dipole antenna, as shown in Figure 1.

Figure 1. 3GPP Rel-15 UE antenna gain patterns: a) Isotropic b) Dipole

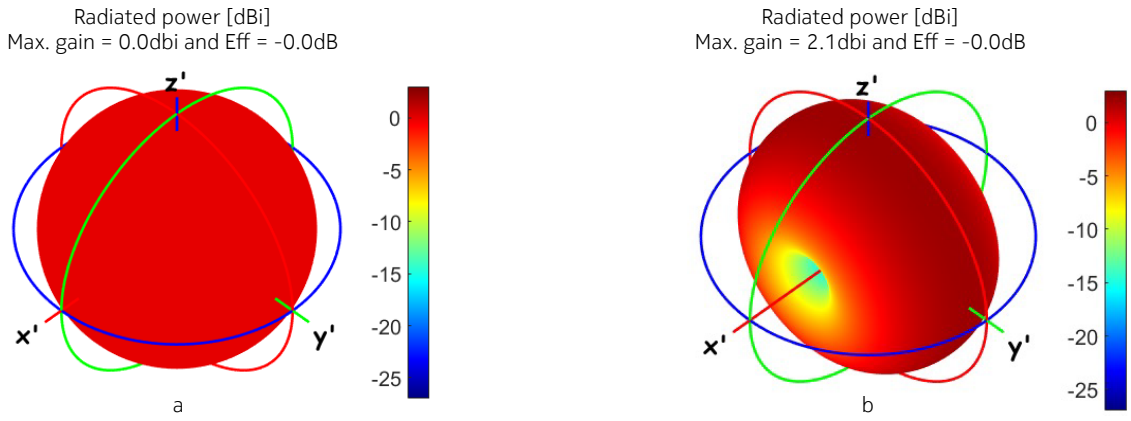

Performing LLS and/or SLS simulation with the isotropic radiator, the antenna-induced effects of the UE are removed for single antenna port (AP) operation. In addition, assuming uniform radiation patterns for all APs will result in too optimistic combined antenna gain values. While this method may be suitable for specific simulation campaigns, it does not necessarily yield realistic results, as the characteristics of antennas integrated into handheld devices, such as smartphones, deviate significantly from those of isotropic or dipole antennas.

In particular, the UE dipole antenna gain radiation pattern serves as a reasonable approximation for free-space antenna characteristics in early-generation mobile phones with external antennas, primarily those of the 2G era. Nevertheless, this approximation is no longer accurate for modern mobile phones equipped with integrated antennas, which are prevalent in 4th (LTE) and 5th (NR) generation devices. As a result, simulations relying on the isotropic radiator assumption may not accurately reflect the real-world performance of these devices.

Rel-15 3GPP UE antenna placement

First generation mobile phones (1G and 2G) only had one antenna for each supported system band, thus UE antenna placements were less relevant. However, 2x2 DL MIMO was introduced for 3G (Rel-7, 2007) and the two APs at the UE were modeled as two orthogonal APs, as shown in Figure 2a, while 4x4 MIMO was introduced for 4G (Rel-8, 2008) and the UE antenna placement was expanded to a 1x2 dual polarized antenna array configuration with 4 APs, as shown in Figure 2b.

Figure 2. 3GPP antenna placements: a) 3G b) 4G/5G

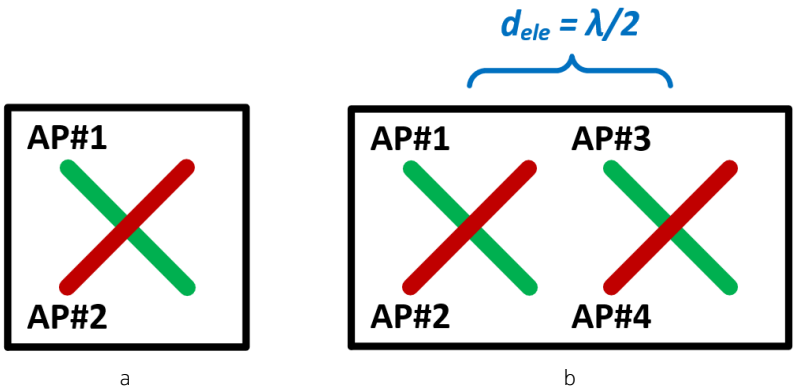

The Rel-15 UE antenna model specified by 3GPP is based on a conventional approach used for gNBs, which typically feature antenna arrays with a half-wavelength electrical distance between uniform linear elements, i.e., a dual polarized uniform linear array (ULA). This ULA model is a suitable approximation for gNBs and other devices with regular antenna arrays, such as fixed wireless access and customer premises equipment network termination units. However, this approach is not well-suited for handheld devices like smartphones, which exhibit antennas with non-uniform antenna characteristics and non-uniform electrical distances between antennas.

In contrast to gNBs, smartphone antennas are often situated along the device's edge, where the chassis serves as the ground plane. The size and individual placement of the antennas significantly influence their characteristics, rendering the aforementioned model unsuitable for this application. As a result, an alternative modeling approach is required in 6G to accurately capture the complex antenna behavior in handheld devices.

Rel-15 3GPP UE antenna polarization

The 3GPP Rel-15 UE antenna model does not directly account for antenna polarizations, as it relies on the assumption of perfect linear orthogonality between pairs of APs arranged in the array configuration. This assumption is based on the premise that two APs share the same phase center offset (PCO) and are perfectly orthogonal regardless of the directivity of the channel, i.e., the angular direction of the incoming power or outgoing signal.

However, this assumption may not hold true in real devices, particularly for handheld phones. In such cases, the antennas are not perfectly orthogonal to any other antennas, and they may not be linearly polarized across all angular directions. Furthermore, each AP will not have similar PCOs, which can lead to polarization-related effects that are not captured by the 3GPP Rel-15 UE antenna model.

Rel-15 3GPP combining of multiple antennas

As legacy radiation patterns are assumed to be uniform and since the same electrical distance between pairs of AP (for example λ/2) is used for all frequencies, all obtained antenna radiation patterns resulting from combining two or more APs will not change over frequency. This is due to the ULA assumption used for the legacy UE antenna model, where the physical distance between the antenna elements changes as a function of the system frequency, i.e., fixed electrical distance of λ/2.

The single AP isotropic radiation pattern is shown in Figure 1a, whereas the combining of isotropic APs (1 and 3 or 2 and 4) spaced with λ/2 and with 90° phase shifts are shown in Figure 3.

Figure 3. Combined dual AP (AP1 & AP3 or AP2 & AP4) radiation patterns for 3GPP Rel-15 UE model a) 0° phase shift b) 90° phase shift c) 180° phase shift d) 270° phase shift

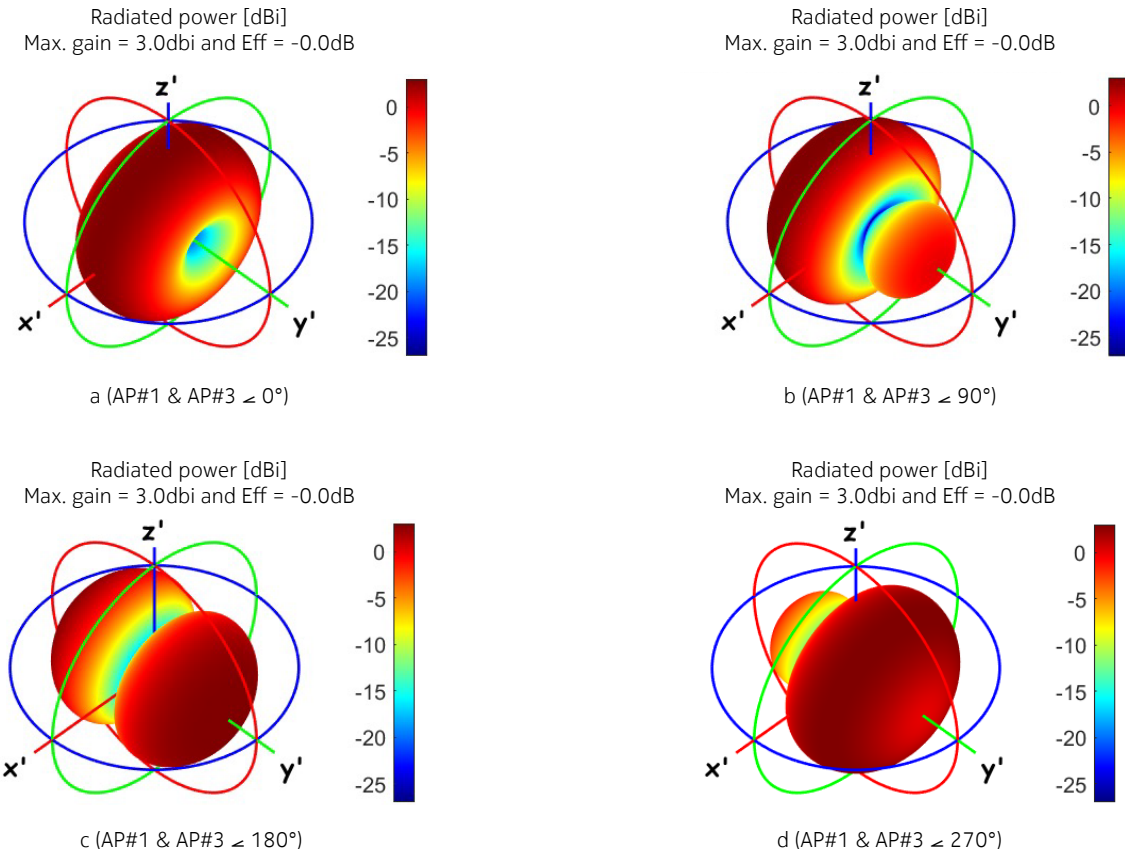

Combing two isotropic antennas spaced with λ/2 electrical length results in well-defined radiation patterns with an increased maximum antenna gain of 3 dB in specific angular directions.

The 3GPP Rel-15 UE antenna assumption described in section 2.1 to section 2.4 are not valid for a handheld device like a smartphone, as mentioned above and explained in detail in the next section.

Nokia 6G smartphone reference model

All the simulated results presented in this whitepaper are based on a 6G reference smartphone implemented with all potential antennas for 6G. The MCAD (mechanical computer-aided design) model of this reference smartphone is shown in Figure 4.

Figure 4. MCAD model of the 6G reference smartphone

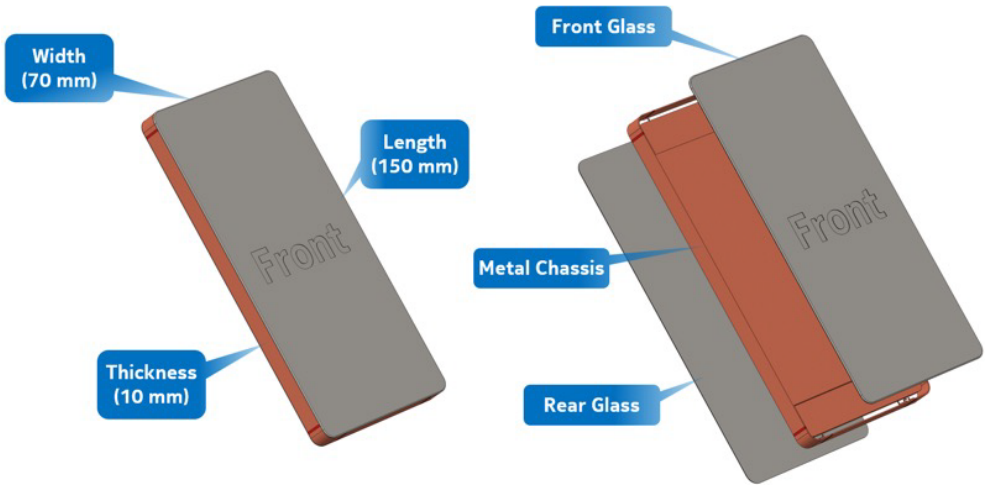

The potential system bands that a 6G smartphone may have to cover can range from 663 MHz to 43.5 GHz. This frequency span is divided into different frequency band groups (FBG) using the definitions shown in Table 1. Each of the FBGs may be required to be covered by multiple different antennas to support downlink (DL) multiple-input multiple-output (MIMO), as DL typically supports more MIMO layers than uplink (UL) for handheld devices.

Table 1. Defined frequency ranges to be covered by the antennas

Frequency range	MIMO	Frequency range start	Frequency range stop
LB	2	633 MHz	960 MHz
MHB	4	1710 MHz	2690 MHz
eUHB	4	3300 MHz	4200 MHz
6G-1	4	4400 MHz	4800 MHz
6G-2	8	7125 MHz	8400 MHz
6G-3	8	14800 MHz	15350 MHz
FR2-1	2	24250 MHz	29500 MHz
FR2-2	2	37000 MHz	43500 MHz

The physical locations of the 22 antennas are shown in Figure 5 and 6, where the new 6G-1 system band is covered by the same physical antennas that cover the legacy 5G frequency range ultra-high band (UHB), forming a new extended UHB (eUHB) definition. The FR2 (mmWave) antennas are included for completeness, however, FR2 antenna characteristics and performance are not within the scope of this whitepaper.

Figure 5. Physical location of the antennas of the reference MCAD model, part 1.

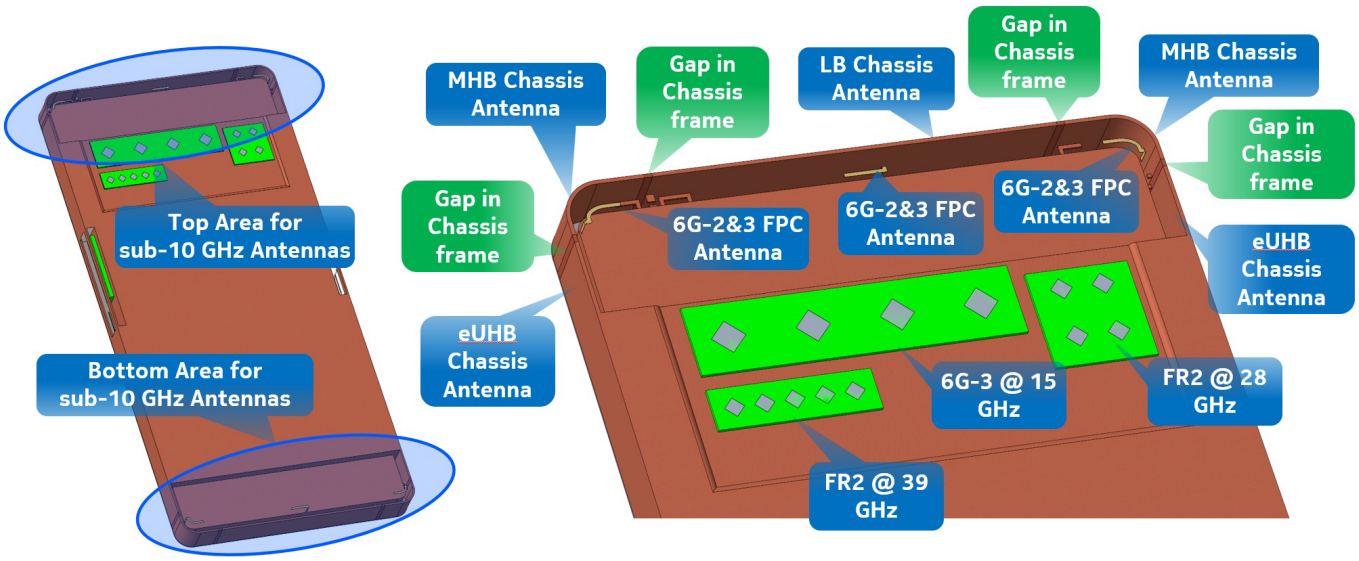

Ant#1	Ant#2	Ant#3	Ant#4	Ant#5	Ant#6	Ant#7	Ant#8	Ant#20	Ant#21	Ant#22
LB Top	MHB Top-left	MHB Top-right	eUHB Top-left	eUHB Top-right	6G-2&3 Top-left	6G-2&3 Top-mid	6G-2&3 Top-right	6G-3	FR2-1	FR2-2

Figure 6. Physical location of the antennas of the reference MCAD model, part 2.

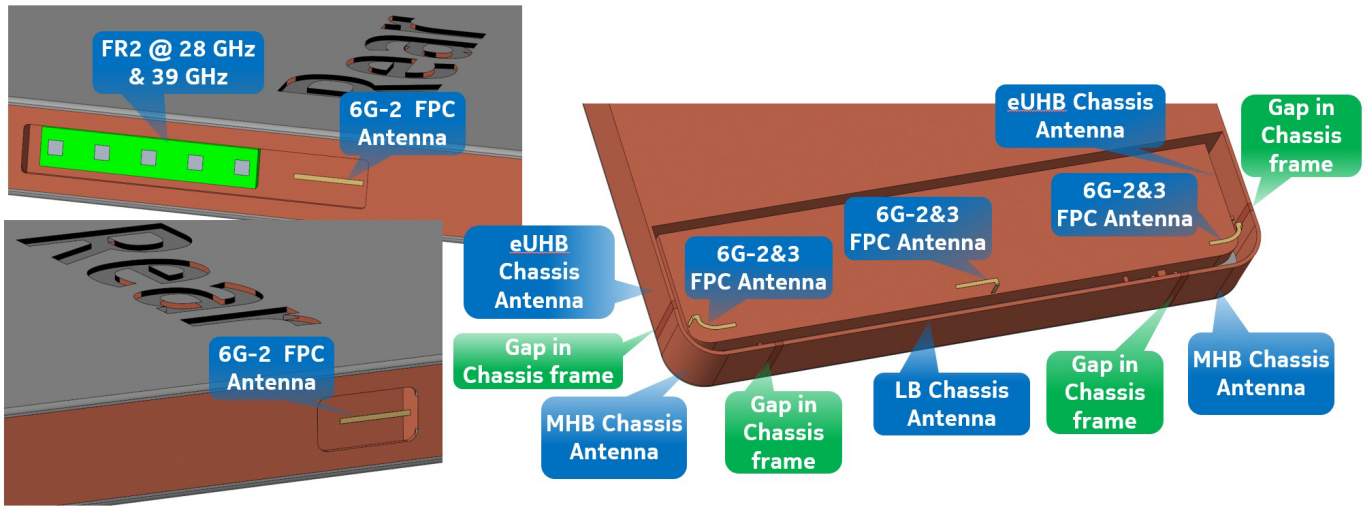

Ant#9	Ant#10	Ant#11	Ant#12	Ant#13	Ant#14	Ant#15	Ant#16	Ant#17	Ant#18	Ant#19
LB Bot	MHB Bot-left	MHB Bot-right	eUHB Bot-left	eUHB Bot-right	6G-2&3 Bot-left	6G-2&3 Bot-mid	6G-2&3 Bot-right	6G-2&3 Side-right	6G-2&3 Side-left	FR2-1&2

The MCAD drawings depicted in Figure 5 and Figure 6 reveal distinct differences in the implementation of antennas for various frequency bands in 6G. Specifically, the low-band (LB), mid/high-band (MHB), and extended ultra-high band (eUHB) antennas are realized as chassis antennas, which are more susceptible to user interaction due to their exposed nature. In contrast, the 6G-2 and 6G-3 antennas are designed as flexible printed circuit (FPC) antennas, mounted internally within the device, thereby maintaining a safe distance from user interactions.

Notably, the introduction of 8x8 DL MIMO capabilities for 6G in the 6G-2 and 6G-3 frequency bands necessitates the inclusion of four additional antennas in the MCAD model. Although 8x8 DL MIMO is not currently anticipated for other frequency ranges in 6G, the 3GPP standard provides a possibility to include eight antennas for all bands, except for the LB frequency range, for the new UE antenna model. To obtain antenna characteristics for these additional antennas, they were tuned to MHB and UHB, leveraging existing band/antenna configurations to derive results.

Reference UE antenna simulations

Electro-magnetic (EM) simulations, using CST [1], of the antenna performance are done under different user-inflicted environmental conditions, like free space and right-hand browse as defined by the Cellular Telecommunications and Internet Association (CTIA) [2], an internally defined dual-hand browsing grip, and for head and hand right side as defined by CTIA. These grips are shown in Figure 7.

Figure 7. Used head and hand phantom grips for the simulations

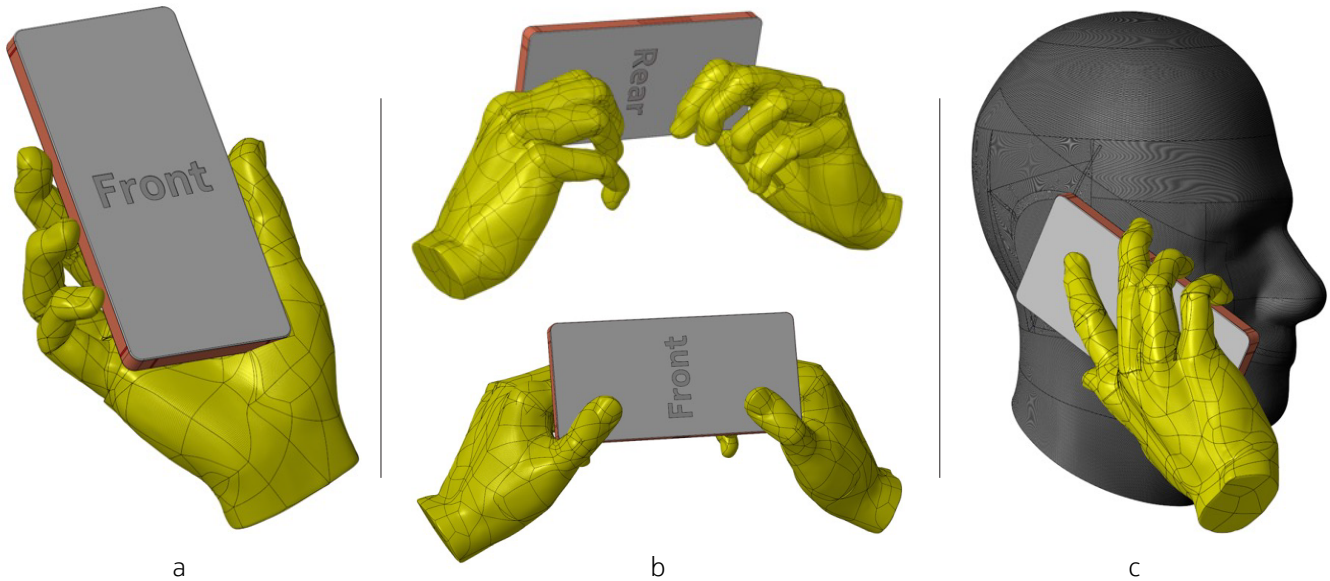

The performance of all the antennas is evaluated through simulations of the four defined use cases and across the following frequencies: 700 MHz, 2000 MHz, 2600 MHz, 3800 MHz, 4600 MHz and 7800 MHz. The electrical properties of the human head and hand, as defined by CTIA, were utilized for the simulations. These properties, denoted as ε' (dielectric constant) and ε'' (dielectric loss factor), are provided for frequencies spanning from 300–6000 MHz, encompassing the majority of the simulated frequencies. However, to accommodate the 7800 MHz frequency, a second-order extrapolation of the CTIA-provided values was performed, as illustrated in Figure 8.

Figure 8. Used second order fit/extrapolation of the CTIA-defined electrical parameter for human head (a) and hand (b)

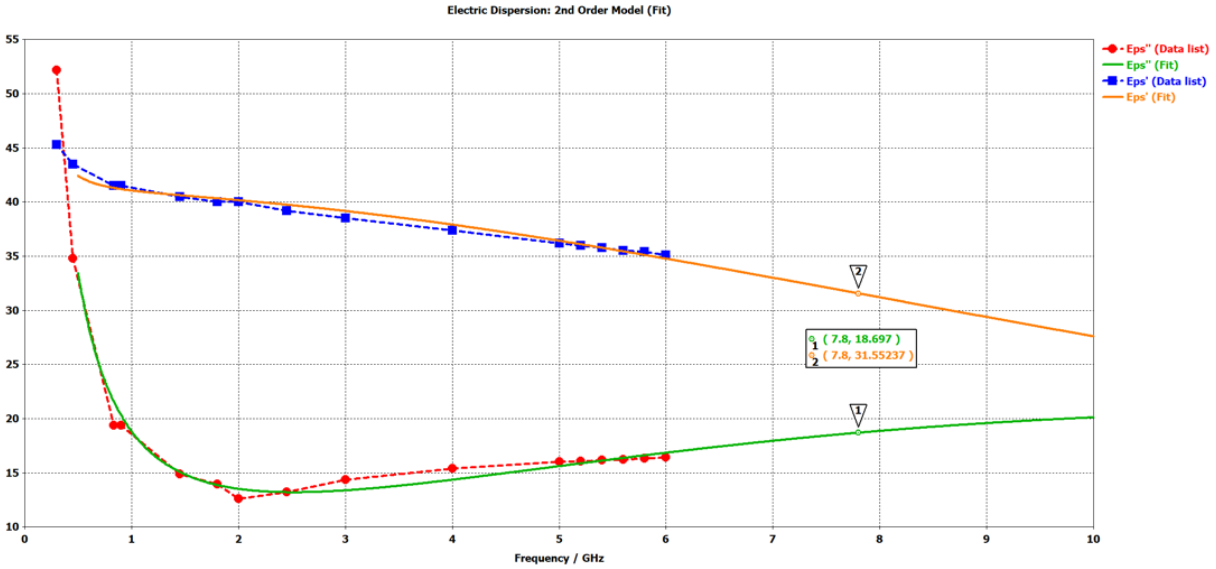

a

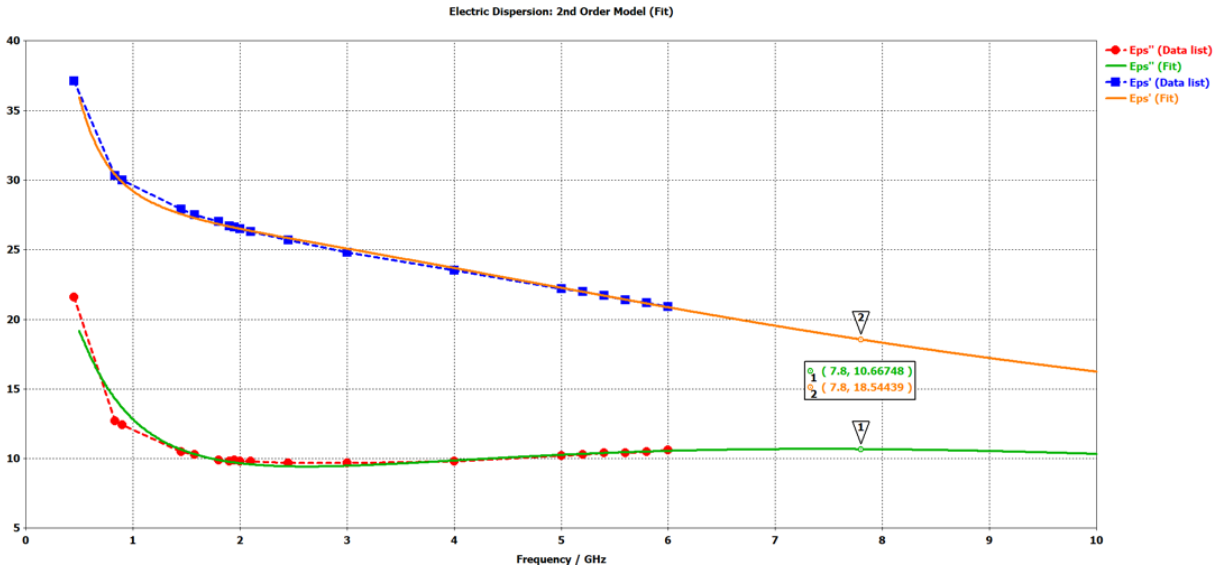

b

The MCAD model was enhanced by incorporating lossy substrates to accurately simulate the absorption loss in the EM simulations. This modification aimed to obtain free-space antenna efficiencies that are comparable to those typically observed in modern high-end smartphones. The electrical parameters utilized for the various materials included in the MCAD model are presented in Table 2, providing a comprehensive understanding of the simulation setup.

Table 2: The electrical parameters used for the different materials included in the MCAD model

Electrical parameters of the used materials	Dielectric constant	Loss tangent	Conductivity
Glass	5.75	0.03	-
Chassis/antennas	-	-	5.8e7 S/m
PC/ABS	2.8	0.007	-
Lossy substrate #1	2.8	0.1	-
Lossy substrate #2	2.8	0.25	-
Lossy substrate #3	1.1	0.4	-
CTIA hand phantom	CTIA specification (See Figure 8a)		
CTIA head phantom	CTIA specification (See Figure 8b)		
CTIA head shell	CTIA specification		

The obtained EM simulation results using the parameters listed in Table 2 were directly used to specify the near-field attenuation values for the new Rel-19 3GPP Near-Field Blockage Model for handheld devices (see final section).

Antenna characteristics in free space

The free-space characteristics of the antennas implemented on the Nokia 6G reference smartphone are shown in the following sections.

Radiation patterns for free space

The free-space radiation patterns are only presented for a single antenna due to the symmetrical nature of the MCAD model along all planes (front, side and top). As a result, the simulated radiation patterns exhibit mirrored versions of each other. Specifically, the second radiation pattern is a mirror image along the top plane, while the third and fourth radiation patterns for MHB and UHB are mirrored versions of the first and second radiation patterns along the side plane. This symmetrical approach approximates real-world smartphone antennas as the radiation patterns are not perfectly symmetrical versions of each other. However, the overall shape of the radiation patterns is primarily determined by the physical placement of the antenna relative to the phone chassis, such as the top and bottom edge center for LB and the four corners (MHB and UHB). Thus, the real-world radiation pattens will have some symmetrical antenna characteristics.

Figure 9. Free-space radiation patterns for one antenna on Nokia's reference 6G smartphone: a) at 900 MHz b) at 2000 MHz c) at 2600 MHz d) at 3800 MHz e) at 4600 MHz f) at 7800 MHz

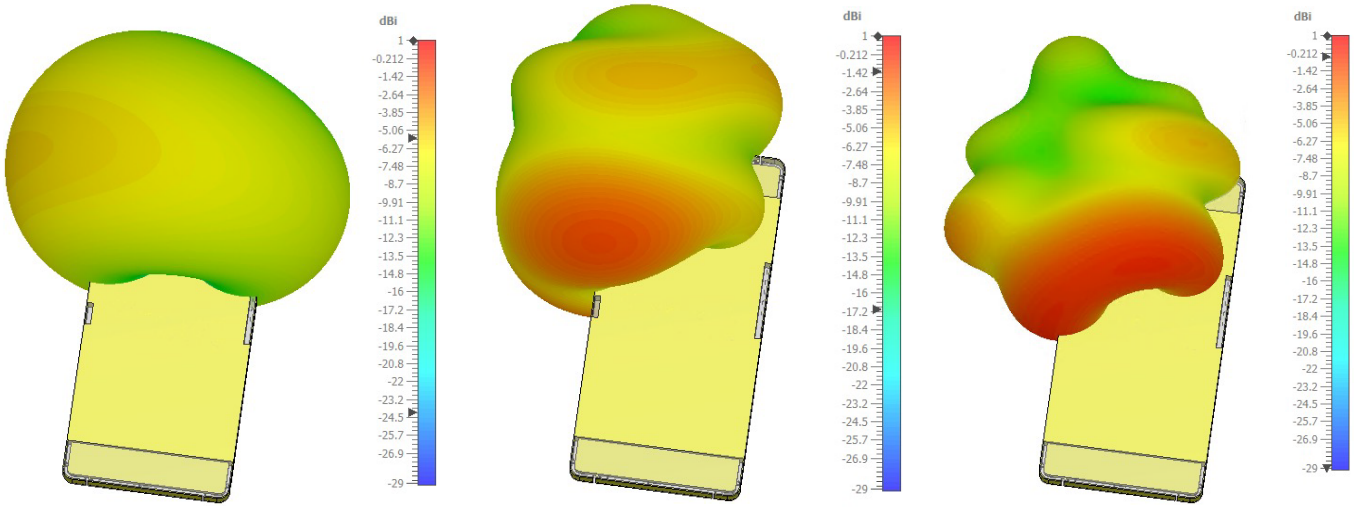

a (900 MHz @ Ant#1) b (2000 MHz @ Ant#2) c (2600 MHz @ Ant#2)

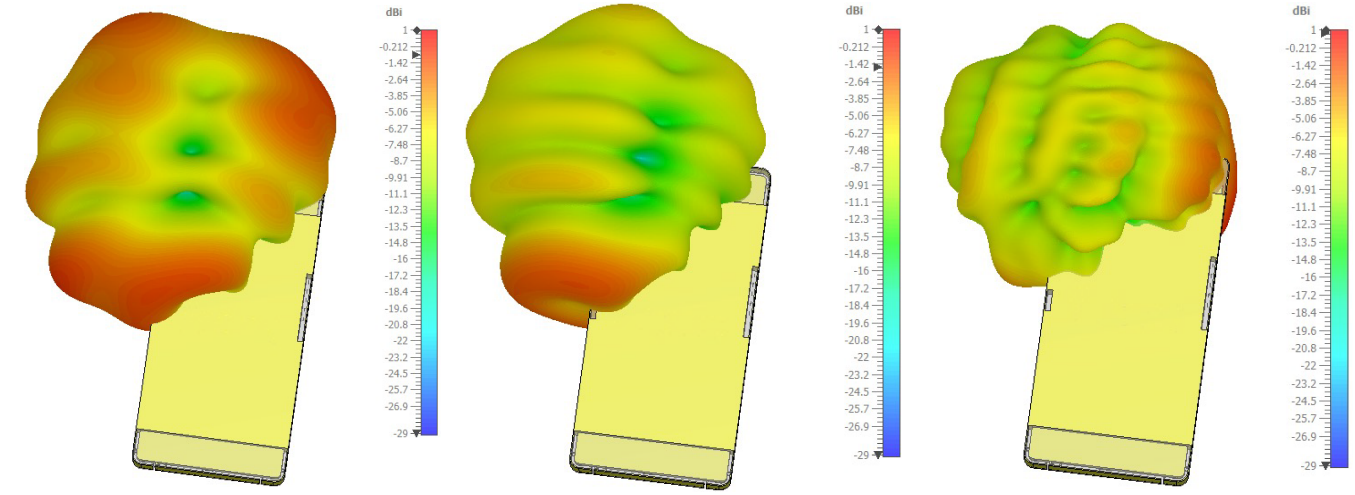

d (3800 MHz @ Ant#2) e (4600 MHz @ Ant#2) f (7800 MHz @ Ant#2)

It is obvious that the radiation patterns on a handheld device are far from isotropic and their maximum antenna gains are in different angular directions. In addition, as the angular direction of the maximum gain is different for each of the antennas, the delta antenna gain values between sets of antennas will also change as a function of angular direction, which is not the case when assuming uniform antennas. This is illustrated in Figure 10, where the maximum gain difference between the best and worst antennas out of the four antennas are plotted for different angular directions at 1° granularity.

Figure 10. The maximum antenna gain difference between four antennas for different angular directions on Nokia's reference 6G smartphone

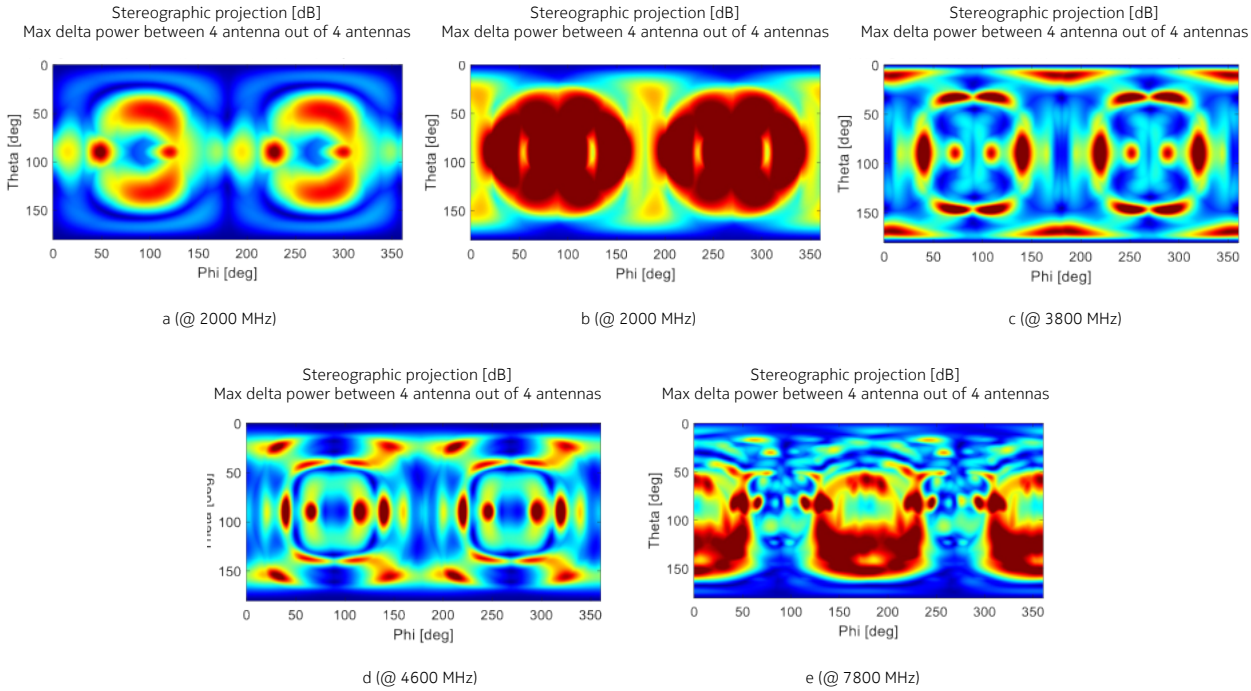

It's clear from Figure 10 that antenna gain imbalances of more than 10 dB are not uncommon, and the angular directions having more than 10 dB antenna gain imbalance (upper truncate value of the plots) change with frequency.

Adding the user grips can increase the antenna gain imbalance to more than 30 dB as illustrated with the following complementary cumulative distribution function (CCDF) curves of the antenna gain imbalance for free-space, CTIA right-hand browsing grip, Nokia dual-hand browsing grip, and CTIA head and hand, right side. More detailed results analyzing the influence of user grips on antenna characteristics are presented in the sections below on antenna characteristics for CTIA right-hand browsing and CTIA head and hand, right side.

Figure 11. CCDF plot of the maximum antenna gain difference between four antennas for different angular directions on Nokia's reference 6G smartphone: a) free space b) CTIA right-hand browsing grip c) Nokia dual-hand browsing grip d) CTIA head and hand, right side

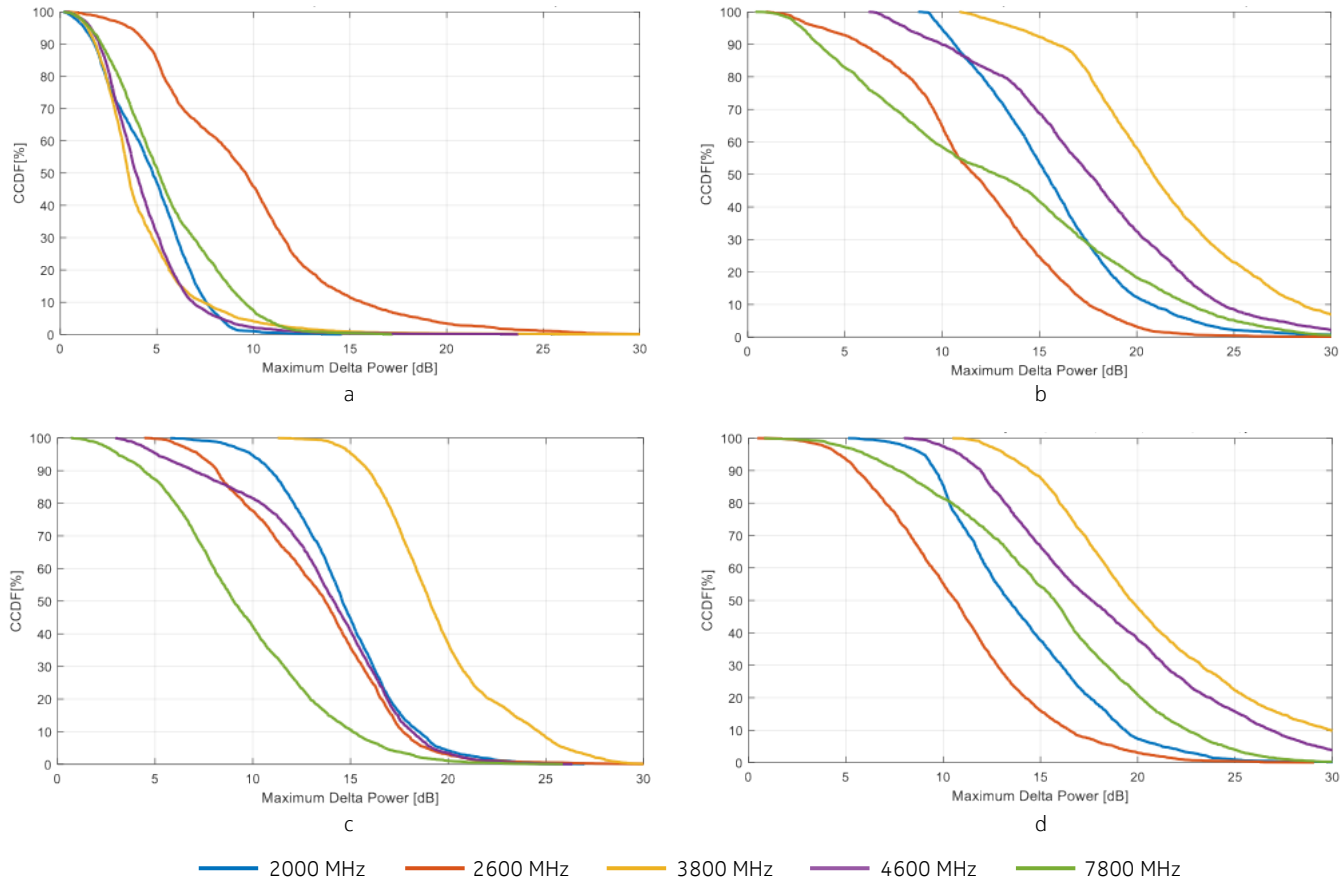

Even at the 50th percentile antenna gain, imbalances between 10 to 20 dB can be expected when the user is holding the phone. This imbalance will impact simulated SLS and LLS performance results when evaluating MIMO (DL and UL), coverage, interference, mobility, etc. and must be included in a new UE model for handheld devices.

Antenna directivity for free space

The radiation patterns of antennas implemented on a smartphone are far from omnidirectional, as shown in the previous section ("Radiation patterns for free space"). The simulated directivity (maximum lossless gain compared to an isotropic antenna) of the antenna implemented on the Nokia 6G reference smartphone are shown in Table 3 for different frequencies. Only one directivity value is shown for each frequency band, as the antennas operating at each frequency have similar directivities, due to the symmetry of the MCAD model.

Table 3. Free space directivity of the antennas at different frequencies

	Simulated antenna directivity for free space [dBi]							
	Top left	Side left	Bot left	Bot mid	Bot right	Side right	Top right	Mid right
700 MHz	-	-	-	3.2	-	-	-	3.3
2000 MHz	5.3	3.6	4.5	4.0	5.3	3.4	4.5	4.5
2600 MHz	6.0	3.2	6.0	5.2	6.0	3.3	6.0	4.8
3800 MHz	3.5	3.9	3.5	3.2	3.5	4.0	3.5	3.3
4600 MHz	5.4	4.2	5.4	5.3	5.3	4.3	5.4	5.1
7800 MHz	7.3	4.9	7.1	5.4	7.0	4.3	6.9	5.7

Directivities between 3.2 dBi and 7.3 dBi can be expected for antennas implemented on a smartphone in free space, when the device is not affected by the user.

Efficiencies for free space

To align with the antenna efficiency characteristics of modern high-end smartphones, the free-space efficiencies of the Nokia reference smartphone have been intentionally reduced through the incorporation of lossy materials in the EM simulations. This deliberate reduction is a result of the 3GPP requirements to support 4x4 MIMO for most MHB and UHB frequencies, the need for global roaming capabilities, and the demand for edge-to-edge displays and thin industrial designs.

The resulting free-space efficiencies for the Nokia reference smartphone are presented in Table 4, ranging from -4.2 dB to -8.8 dB. These values reflect the high-loss antenna characteristics estimated from public compliance certification measurements, like those published by the Federal Communication Commission (FCC).

Table 4. Simulated antenna efficiencies for free space from 700–7800 MHz

	Efficiency for free space [dB]							
	Top left	Side left	Bot left	Bot mid	Bot right	Side right	Top right	Mid right
700 MHz	-	-	-	-8.8	-	-	-	-8.8
2000 MHz	-6.6	-7.6	-6.4	-6.5	-6.7	-7.7	-6.4	-6.6
2600 MHz	-6.5	-7.2	-7.0	-6.1	-6.4	-7.2	-6.8	-6.7
3800 MHz	-4.2	-4.9	-4.2	-4.0	-4.2	-4.8	-4.1	-4.3
4600 MHz	-7.1	-7.8	-7.0	-6.8	-6.7	-7.9	-6.7	-6.9
7800 MHz	-6.4	-8.1	-6.5	-7.2	-6.3	-7.8	-6.5	-7.3

The disparity in efficiencies among antennas operating at the same frequency is primarily attributed to two factors. First, mutual coupling between the distinct antennas is influenced by the physical arrangement of the antenna elements and the location of the antenna feed point. Second, the Q-factor of each antenna (bandwidth relative to the center frequency) also plays a significant role in determining its efficiency. Specifically, the reduced volume available for antennas positioned on the side of the phone results in a higher Q-factor (lower bandwidth), leading to decreased efficiencies (higher capacitive coupling to the ground plane, i.e., the phone chassis) compared to antennas located at the corners of the phone, where a larger volume is available.

Polarizations characteristics of the radiation patterns

The antenna radiation patterns in Figure 9 represented the total absolute gain of the antenna located at the top left corner of the phone. However, it is essential to note that the total absolute gain is comprised of two orthogonal field components: Theta (θ) and Phi (ϕ). The antenna gain values in Figure 9 are only valid for perfect polarization alignment between the field components of the antenna and the channel/ environment.

To provide a more comprehensive understanding of the antenna's radiation behavior, Figure 12 (a–c) presents the total gain and the two orthogonal field components (θ and ϕ) in a spherical coordinate system (x, y and z), where the field components are perpendicular to the z-axis and aligned with the x- and y-axes, respectively. Figure 12a shows the total gain of Ant#2 at 2600 MHz, which is a superposition of the θ and ϕ field components depicted in Figure 12b and 12c.

The radiation patterns of the θ and ϕ field components of the antenna are dynamic and depend on the alignment to the θ and ϕ field components of the channel for a given angular direction. In contrast, the total gain pattern remains constant. This polarization-dependent behavior is crucial for understanding the antenna's performance in various channel environments and for optimizing antenna design to achieve optimal performance.

Figure 12. Radiation patterns of the Theta and Phi polarization components for Ant#3 at 2000 MHz: a) total gain plot b) Theta Field component plot c) Phi Field component plot

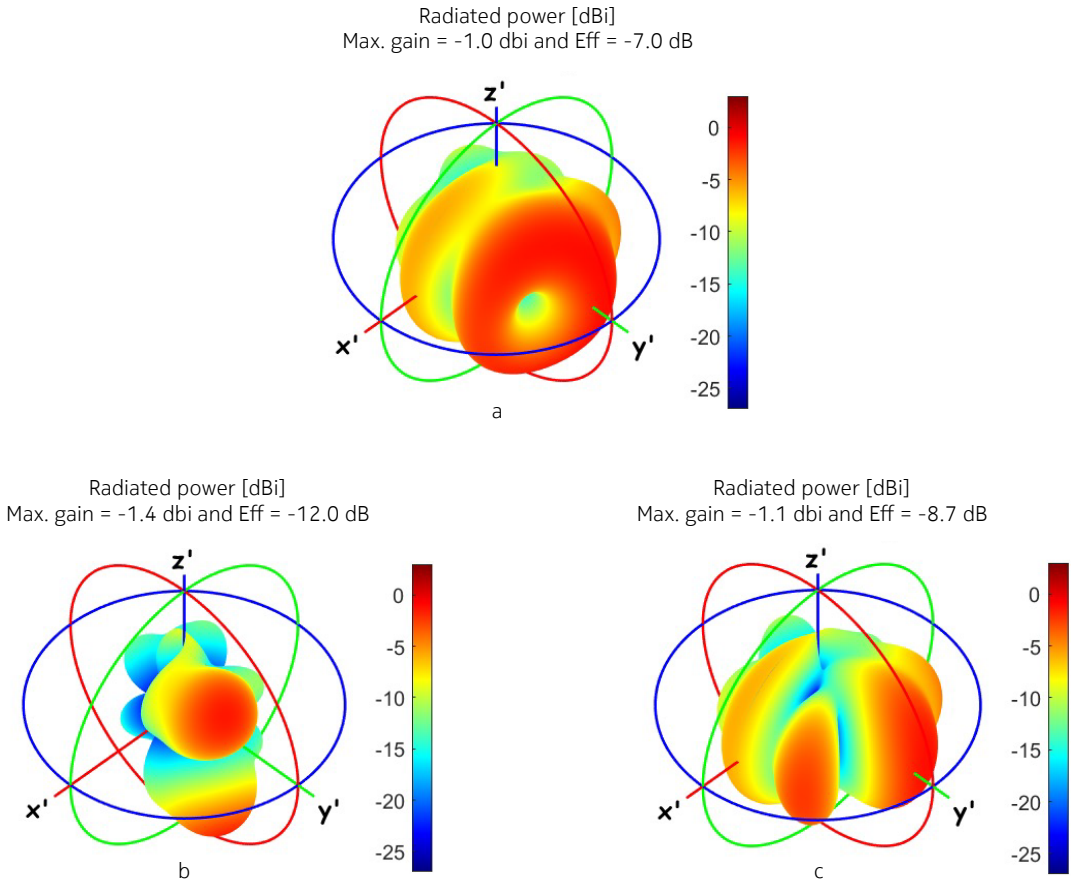

The dynamic behavior of the θ and ϕ field components can be mitigated by implementing antennas with orthogonal dual-polarized elements. Such elements can adaptively align their polarization characteristics to the channel polarization in the digital domain, assuming that each dual-polarized element has its own receiver/transmitter. Adaptive polarization alignment enables theoretical full power transfer, as indicated by the radiation pattern of the total antenna gain.

UE antennas, however, typically employ single-feed designs with predominantly one-dimensional shapes, often located along the device's edge. These single-feed antennas predominantly exhibit a single linear polarized field component, which can be elliptical in certain angular directions and frequencies, "seeing" some power from both θ and ϕ field components. This is illustrated by the stereographic projection in Figure 13b, where lines represent linear polarization, and circles represent circular polarization per direction.

In practice, UE antennas are unlikely to exhibit perfect linear or circular polarization, but rather an elliptical polarization with either right-hand-side (blue) or left-hand-side (red) rotation. This polarization characteristic can impact the antenna's performance and is an important consideration in UE antenna design.

Figure 13. Polarization state of the total gain plot: a) total gain plot b) polarization state plot

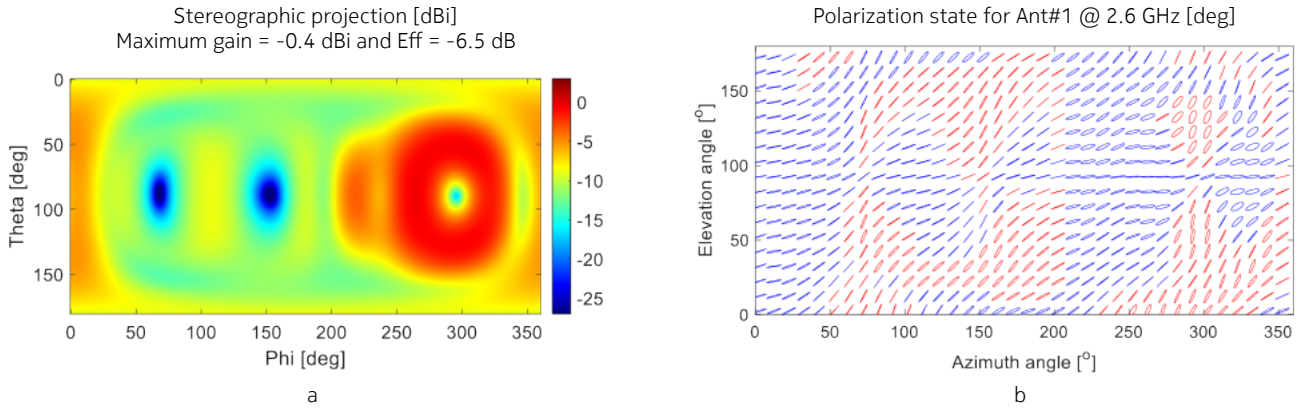

As such, an antenna on a UE will only have full power transfer if the polarization characteristics of the UE antenna and the channel are perfectly aligned for a given angular direction, which is very unlikely.

Antenna characteristics for CTIA right-hand browsing

The antenna characteristics of the antennas implemented on the Nokia 6G reference smartphone when affected by a single-hand browsing grip are shown in the following three sections. The used CTIA hand phantom is shown in Figure 7a.

Radiation patterns for CTIA right-hand browsing

As depicted in Figure 14, the radiation patterns of the four corner-mounted antennas operating at 3800 MHz are no longer symmetrical when subjected to the CTIA-defined single-hand browsing grip.

Figure 14. Antenna radiation patterns at 3800 MHz including CTIA-specified right-hand browsing grip

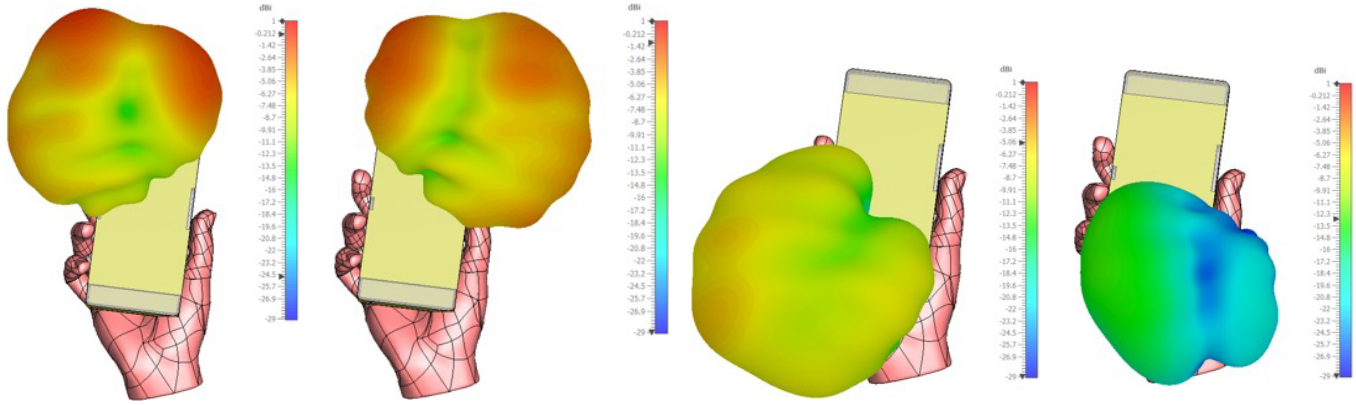

Specifically, the two bottom-mounted antennas exhibit significant changes in their radiation patterns, as evident from the altered shape and color (indicative of reduced power) compared to the free-space simulations. Conversely, the two top-mounted antennas remain largely unaffected, displaying radiation patterns that are similar to those obtained in free-space conditions. These findings highlight the importance of considering the effects of user interaction on antenna performance for handheld devices when performing SLS and LLS simulations.

Antenna directivity for CTIA right-hand browsing

As the top-mounted antennas remained largely unaffected by the grip, their directivities remained comparable to those simulated in free-space conditions (refer to Table 3).

In contrast, the bottom-mounted antennas directly impacted by the hand exhibit an increase in directivity due to the significant influence of the hand on the antenna's characteristics.

Table 5. Directivity of the antennas impacted by CTIA right-hand browsing phantom, 700–7800 MHz carrier frequencies

	Simulated antenna directivity for CTIA right-hand browse [dBi]							
	Top left	Side left	Bot left	Bot mid	Bot right	Side right	Top right	Mid right
700 MHz	-	-	-	-4.3	-	-	-	3.7
2000 MHz	3.9	4.3	6.5	5.9	6.2	3.4	3.0	3.0
2600 MHz	5.2	4.4	6.6	6.3	6.1	4.0	4.9	3.0
3800 MHz	4.4	5.1	5.0	5.9	6.2	6.0	3.9	4.6
4600 MHz	2.9	5.1	4.4	5.0	7.9	6.0	2.5	3.7
7800 MHz	7.9	5.5	7.9	7.1	9.9	7.6	6.7	5.5

It is essential to note, however, that this increase in directivity does not necessarily translate to an equivalent increase in maximum antenna gain, as the hand's effect also leads to decreased antenna efficiency, which must be taken into account.

The phantom grip influence on the directivity and efficiency of the individual antennas is not uniform, which will result in an increased antenna gain imbalance for some angular directions as previously shown in Figure 11b.

Antenna efficiencies for CTIA right-hand browsing

The simulated antenna efficiencies, including the CTIA-specified right-hand browsing grip, are shown in Table 6.

Table 6. Antenna efficiencies impacted by CTIA right-hand browsing, 700–7800 MHz carrier frequencies

	Efficiency for CTIA right-hand browse [dB]							
	Top left	Side left	Bot left	Bot mid	Bot right	Side right	Top right	Top mid
700 MHz				-22.4				-11.2
2000 MHz	-6.9	-11.5	-9.7	-14.0	-20.8	-17.1	-6.8	-6.9
2600 MHz	-8.1	-12.4	-11.0	-12.2	-17.4	-14.4	-8.3	-8.2
3800 MHz	-4.7	-9.2	-7.6	-13.2	-22.8	-16.3	-4.9	-4.7
4600 MHz	-8.0	-11.2	-9.5	-14.5	-20.5	-16.5	-7.5	-7.5
7800 MHz	-6.8	-12.1	-9.7	-13.3	-12.7	-17.7	-6.8	-7.8

The decrease in antenna efficiency between free space and the CTIA right-hand browsing grip is shown in Table 7, which shows a high decrease for antennas (bottom- and side-mounted antennas) directly affected by the hand grip.

Table 7. Δ Efficiency for free space and CTIA right-hand browsing, 700–7800 MHz carrier frequencies

	Δ Efficiency for free space and CTIA right-hand browse [dB]							
	Top left	Side left	Bot left	Bot mid	Bot right	Side right	Top right	Top mid
700 MHz				-13.6				-2.4
2000 MHz	-0.3	-3.9	-3.3	-7.5	-14.1	-9.4	-0.1	-0.3
2600 MHz	-1.6	-5.2	-4.0	-6.1	-11.0	-7.2	-1.5	-1.5
3800 MHz	-0.5	-4.3	-3.4	-9.2	-18.6	-11.5	-0.8	-0.4
4600 MHz	-0.9	-3.4	-2.5	-7.7	-13.8	-8.6	-0.8	-0.6
7800 MHz	-0.4	-4.0	-3.2	-6.1	-6.4	-9.9	-0.3	-0.5
Average (1.0–8.4 GHz)	**-0.7**	**-4.1**	**-3.3**	**-7.2**	**-10.8**	**-9.1**	**-0.7**	**-0.6**

An average efficiency value is derived for each antenna for simulated results obtained at frequencies from 1–8.4 GHz. These values are used later for a new near-field blockage model (see final section, “User contribution to near-field blockage”).

Antenna characteristics for Nokia-defined dual-hand browsing

The characteristics of the antennas implemented on the Nokia 6G reference smartphone when affected by a dual-hand browsing grip are presented in the following three sections. However, as no official hand grip has been specified for a dual-hand browsing grip, a Nokia-defined dual-hand browsing grip (see Figure 7b) has been used to simulate the performance of smartphones when the user is holding the phone using both hands.

Radiation patterns for Nokia-defined dual-hand browsing

As depicted in Figure 15, the radiation patterns of the four corner-mounted antennas operating at 3800 MHz are no longer symmetrical when subjected to the Nokia-defined dual-hand browsing grip.

Figure 15. Antenna radiation patterns at 3800 MHz including the Nokia-defined dual-hand browsing grip

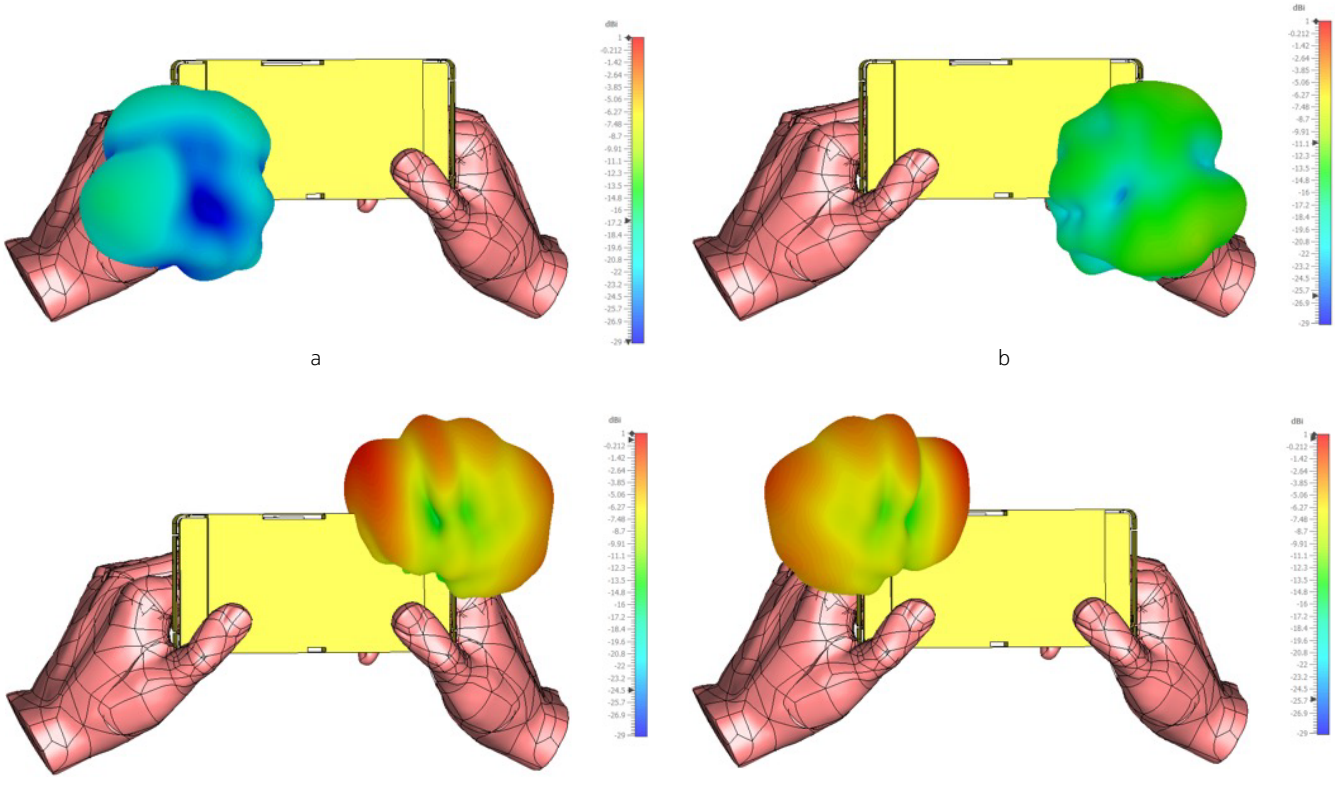

It is clear that the two left-side-mounted antennas (lower side in this figure after a counterclockwise rotation of the phone from portrait to landscape mode) are affected by the user grip, as the shape and color (power reduction) of the radiation patterns have changed compared to those obtained in free space. The two antennas on the right side of the phone (top side in this figure) are almost unaffected and have similar radiation patterns to free space.

Antenna directivity for Nokia dual-hand browsing

As the left-side-mounted antennas remained largely unaffected by the grip, their directivities remained comparable to those simulated in free-space conditions (refer to Table 3).

In contrast, the right-side-mounted antennas directly impacted by the hand exhibited an increase in directivity due to the significant influence of the hands on the antennas' characteristics.

Table 8. Directivity of the antennas at different frequencies when including Nokia dual-hand browsing phantom

	Simulated antenna directivity for Nokia dual-hand browsing [dBi]							
	Top left	Side left	Bot left	Bot mid	Bot right	Side right	Top right	Mid right
700 MHz	-	-	-	3.5	-	-	-	4.6
2000 MHz	5.2	3.1	4.9	3.9	4.6	3.6	3.9	5.6
2600 MHz	4.0	4.1	4.5	4.8	6.3	3.3	6.4	4.1
3800 MHz	5.5	4.4	5.6	4.8	5.8	4.4	5.9	5.1
4600 MHz	6.2	5.4	6.0	5.8	5.5	4.8	5.5	5.7
7800 MHz	7.9	5.9	7.5	4.9	5.5	5.0	6.1	5.0

It is essential to note, however, that this increase in directivity does not necessarily translate to an equivalent increase in maximum antenna gain, as the hand's effect also leads to decreased antenna efficiency, which must be considered.

The dual-hand phantom grip's influence on the directivity and efficiency of the individual antennas is not uniform, which will result in an increased antenna gain imbalance for some angular directions, as previously shown in Figure 11c.

Efficiencies for Nokia dual-hand browsing

The simulated antenna efficiencies including the Nokia-defined dual-hand browsing grip are shown in Table 9.

Table 9. Simulated antenna efficiencies for Nokia dual-hand browsing from 700–7800 MHz

	Efficiency Nokia dual-hand browse [dB]							
	Top left	Side left	Bot left	Bot mid	Bot right	Side right	Top right	Top mid
700 MHz				-14.6				-14.4
2000 MHz	-20.1	-8.6	-19.0	-13.5	-8.8	-9.8	-8.1	-14.3
2600 MHz	-18.0	-8.1	-18.0	-12.4	-8.0	-8.8	-8.2	-13.8
3800 MHz	-22.2	-5.7	-22.3	-9.8	-5.4	-6.3	-5.3	-11.0
4600 MHz	-21.7	-8.8	-22.0	-11.8	-7.5	-9.2	-7.1	-12.6
7800 MHz	-12.8	-9.8	-12.2	-11.7	-8.9	-8.3	-8.6	-11.7

The decrease in antenna efficiency between free space and the Nokia dual-hand browsing grip is seen in Table 10, which shows a high decrease for the antennas (left corner antennas and the two mid-antennas in the top and bottom), because they are directly affected by the hand grip.

Table 10. Δ efficiency free space and Nokia dual-hand browsing from 700–7800 MHz

	Δ efficiency free space and Nokia dual-hand browse [dB]							
	Top left	**Side left**	**Bot left**	**Bot mid**	**Bot right**	**Side right**	**Top right**	**Top mid**
700 MHz				-5.8				-5.6
2000 MHz	-13.5	-1.0	-12.6	-7.0	-2.1	-2.1	-1.7	-7.7
2600 MHz	-11.5	-0.9	-11.0	-6.3	-1.6	-1.6	-1.4	-7.1
3800 MHz	-18.0	-0.8	-18.1	-5.8	-1.2	-1.5	-1.2	-6.7
4600 MHz	-14.6	-1.0	-15.0	-5.0	-0.8	-1.3	-0.4	-5.7
7800 MHz	-6.4	-1.7	-5.7	-4.5	-2.6	-0.5	-2.1	-4.4
Average (1.0–8.4 GHz)	**-11.0**	**-1.1**	**-10.6**	**-5.6**	**-1.5**	**-1.4**	**-1.3**	**-6.2**

The impact of the near-field radiation propagation intensity is dependent on the wavelength, whereby an antenna operating at lower frequencies will be more affected by objects at specific physical distances. This is reflected in the results where antennas not directly covered by the hand grip (right-side antennas) increase in efficiency as the frequency increases. However, the antennas at 7800 MHz are implemented as monopole antennas using the rear-side face of the chassis as the ground plane, which means they will radiate more energy in the rear-side direction of the device, towards the majority of the hand phantom in this grip scenario This effect is seen in the efficiency results where, for example, the top right and top left have decreased efficiency compared to, for example, those at 4600 MHz.

An average efficiency value is derived for each antenna for simulated results obtained at frequencies from 1–8.4 GHz. These values are used later for a new near-field blockage model (see final section, “User contribution to near-field blockage”).

Antenna characteristics for CTIA head and hand, right side

The antenna characteristics of the antennas implemented on the Nokia 6G reference smartphone when affected by the head and hand in talk mode are shown in the following three sections. The CTIA head and hand, phantom right side used in this analysis are shown in Figure 7c.

Radiation patterns for CTIA head and hand right

As depicted in Figure 16, the radiation patterns of the four corner-mounted antennas operating at 3800 MHz are no longer symmetrical when subjected to the CTIA-defined head and hand right side phantoms.

Figure 16. Antenna radiation patterns at 3800 MHz including the CTIA-defined head and hand, right side

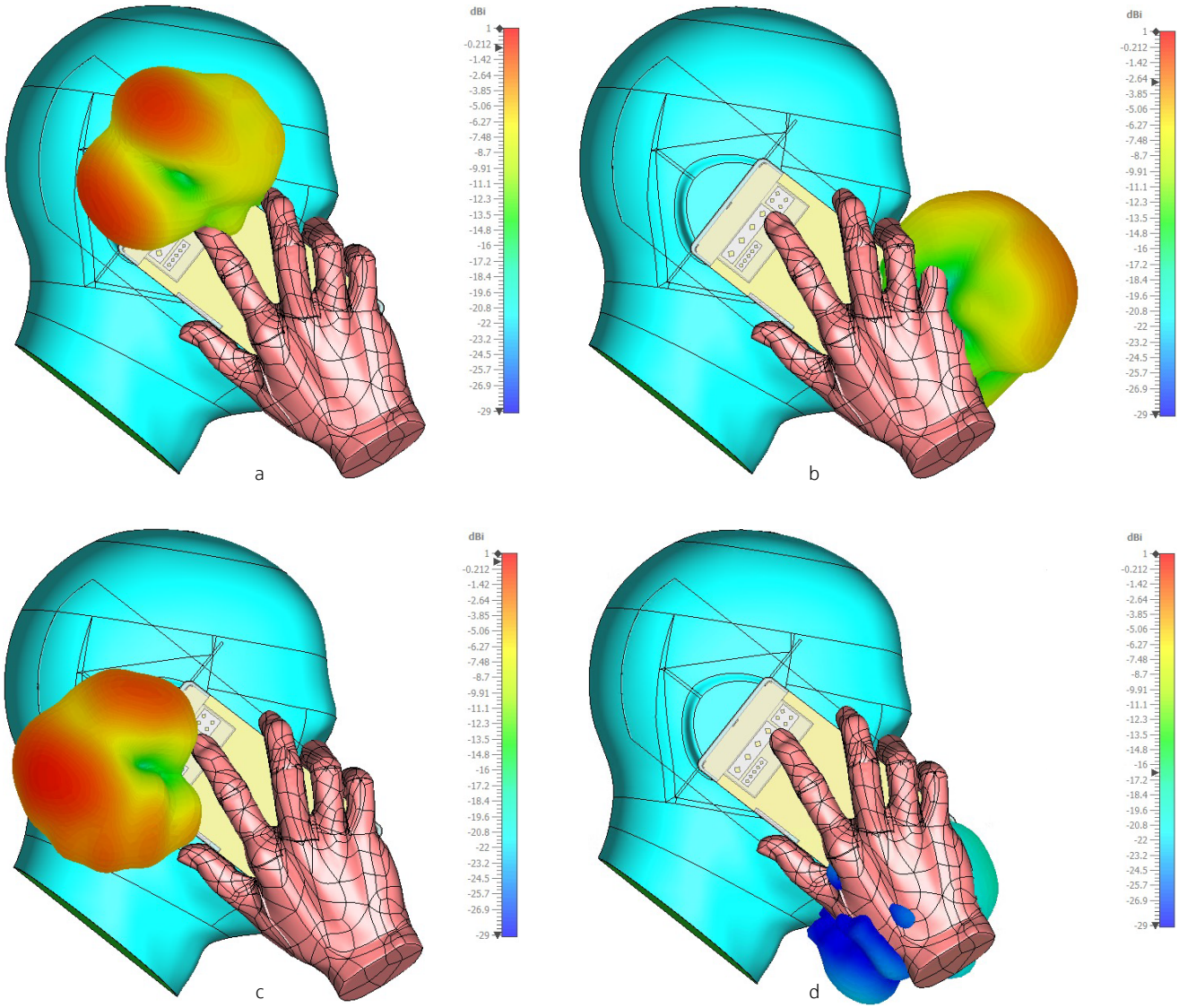

All antennas exhibit significant changes in their radiation patterns, as evident from the altered shape and color (indicative of reduced power) compared to the free-space simulations. In addition, the bottom-mounted antennas are more affected than the top-mounted antennas.

Antenna directivity for CTIA head and hand, right side

As all the antennas are affected by the phantoms, the directivity values are also different compared to the directivity values obtained for free space (see Table 3).

Table 11. Directivity of the antennas at different frequencies when including the CTIA head and hand, right-side phantoms

	Simulated antenna directivity for CTIA head and hand, right side [dBi]							
	Top left	Side left	Bot left	Bot mid	Bot right	Side right	Top right	Mid right
700 MHz	-	-	-	3.8	-	-	-	4.2
2000 MHz	4.8	6.6	5.2	5.8	7.1	6.1	6.9	6.9
2600 MHz	5.5	6.1	6.4	5.2	7.3	6.8	8.6	7.0
3800 MHz	5.1	6.9	7.1	6.1	7.8	8.5	7.4	7.9
4600 MHz	5.5	6.9	9.5	6.1	7.8	9.4	5.8	7.6
7800 MHz	8.8	7.4	11.3	8.3	9.5	11.2	8.0	8.5

It is essential to note, however, that this increase in directivity does not necessarily translate to an equivalent increase in maximum antenna gain, as the hand-and-head effect also leads to decreased antenna efficiency, which must be considered.

The phantom's influence on the directivity and efficiency of the individual antennas is not uniform, which will result in an increased antenna gain imbalance for some angular directions as previously shown in Figure 11d.

Efficiencies for CTIA head and hand, right side

The simulated antenna efficiencies including the Nokia-defined dual-hand browsing grip are shown in Table 12 below.

Table 12. Simulated antenna efficiencies for CTIA head and hand right side from 700–7800 MHz

	Efficiency CTIA head and hand, right side[dB]							
	Top left	Side left	Bot left	Bot mid	Bot right	Side right	Top right	Top mid
700 MHz				-23.9				-13.7
2000 MHz	-11.3	-12.0	-12.1	-15.0	-22.7	-17.5	-10.7	-13.0
2600 MHz	-12.1	-12.9	-12.7	-13.3	-17.0	-15.5	-11.0	-12.1
3800 MHz	-8.2	-9.6	-8.0	-14.2	-24.0	-17.0	-7.0	-8.0
4600 MHz	-10.3	-11.7	-9.9	-15.6	-21.3	-17.3	-8.7	-12.5
7800 MHz	-8.3	-12.8	-10.2	-12.8	-14.0	-19.7	-8.3	-9.1

The decrease in antenna efficiency between free space and the CTIA head and hand, right side is shown in Table 13, which shows a high decrease for antennas (left corner antennas and the two mid antennas in the top and bottom) directly affected by the hand grip and a smaller increase for the antennas only affected by the head.

Table 13. Δ efficiencies for free space and head and hand, right side from 700–7800 MHz

	Δ efficiency free space and CTIA head and hand right side [dB]							
	Top left	**Side left**	**Bot left**	**Bot mid**	**Bot right**	**Side right**	**Top right**	**Top mid**
700 MHz				-15.1				-4.9
2000 MHz	-4.7	-4.4	-5.7	-8.5	-16.0	-9.8	-4.3	-6.4
2600 MHz	-5.6	-5.7	-5.7	-7.2	-10.6	-8.3	-4.2	-5.4
3800 MHz	-4.0	-4.7	-3.8	-10.2	-19.8	-12.2	-2.9	-3.7
4600 MHz	-3.2	-3.9	-2.9	-8.8	-14.6	-9.4	-2.0	-5.6
7800 MHz	-1.9	-4.7	-3.7	-5.6	-7.7	-11.9	-1.8	-1.8
Average (1.0–8.4 GHz)	**-3.7**	**-4.6**	**-4.3**	**-7.8**	**-11.7**	**-10.1**	**-2.9**	**-4.2**

An average efficiency value is derived for each antenna for simulated results obtained at frequencies from 1–8.4 GHz. These values are used later for a new near-field blockage model (see final section, “User contribution to near-field blockage”).

Rel-19 3GPP UE antenna model

The antenna characteristics of the UE model specified in Rel-15 of the 3GPP standard deviate significantly from those typically observed in handheld devices such as smartphones. This discrepancy motivated the proposal for a new UE antenna model for Rel-19, which will be applicable to 6G devices from Rel-20 onwards. The primary objective of this revised model is to align the 3GPP's LLS and SLS simulation methodologies with real-world antenna behavior for handheld devices. Furthermore, a more realistic antenna model will enable the identification of areas within the 3GPP standardization that require updates to enhance overall performance.

Rel-19 3GPP UE antenna pattern

A directive UE reference antenna radiation gain pattern is defined in accordance with the established approach within 3GPP for a single antenna element at a gNB (refer to Table 7.3-1, TS 38.901 [3]). The updated values for the UE reference antenna radiation gain pattern are presented in (Table 14) below.

Table 14. 3GPP Rel-19 antenna radiation pattern for handheld devices

Parameter	Values
Vertical cut of the radiation power pattern (dB)	$A''_{dB}(\theta'', \phi'' = 0°) = -min\left\{12\left(\frac{\theta'' - 90°}{\theta_{3dB}}\right)^2, SLA_V\right\}$ $with\ \theta_{3dB} = 125°, SLA_V = 22.5\ dB\ and\ \theta'' \epsilon\ [-180°, 180°]$
Horizontal cut of the radiation power pattern (dB)	$A''_{dB}(\theta'' = 90°, \phi") = -min\left\{12\left(\frac{\phi''}{\phi_{3dB}}\right)^2, A_{max}\right\}$ $with\ \phi_{3dB} = 125°, A_{max} = 22.5\ dB\ and\ \phi'' \epsilon\ [-180°, 180°]$
3D radiation power pattern (dB)	$A''_{dB}(\theta'', \phi'') = -min\left\{-\left(A''_{dB}((\theta'', \phi'' = 0°) + A''_{dB}(\theta'' = 90°, \phi''))\right), A_{max}\right\}$
Maximum directional gain of an antenna element GE,max	5.3 dBi

Using the 3GPP approach and values from Table 14, a UE reference antenna radiation gain pattern is obtained, as depicted in Figure 17, within the antenna coordinate system (ACS → x'', y'', z'').

Figure 17. UE reference antenna radiation gain pattern

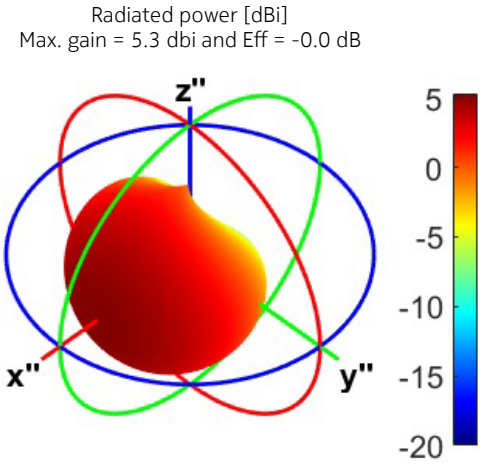

The resulting UE reference antenna radiation gain pattern exhibits a directivity of 5.3 dBi, a 3 dB radiation beamwidth of 125° in both θ and ϕ, and a front-to-back lobe ratio of 22.5 dB.

A comparison of this updated reference antenna radiation gain pattern with the simulation free-space radiation patterns shown in Figure 9 and the directivities from Table 3 reveals that it provides a more accurate approximation than an isotropic radiation pattern.

This improved approximation was one of the key factors in Nokia's initial proposal to modify the UE model in 3GPP.

Rel-19 3GPP UE antenna placements

Eight different antenna candidate location are specified along the edge of a 150 mm x 70 mm reference handheld device form factor, where the maximum antenna gain direction of the UE reference antenna radiation gain pattern is oriented and aligned with the X-axis, the Y-axis or one of two reference diagonal axes with a 25° tilt to the Y-axis, as shown in Figure 18.

Figure 18. Antenna locations and orientations on the handheld form factor

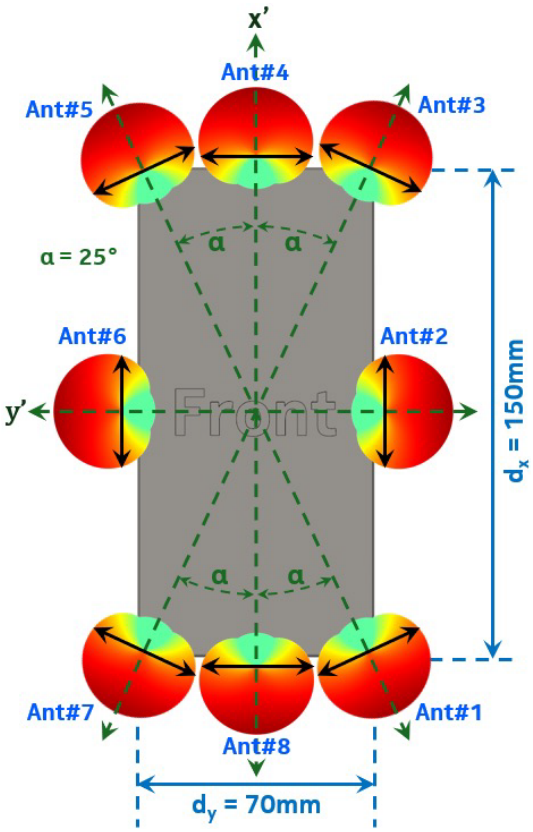

Each of the eight radiation patterns has its maximum gain in different angular directions, reflecting the antenna characteristics observed for antennas implemented on handheld devices like smartphones. The non-uniform physical distances between the antennas result in frequency-dependent antenna combining, as discussed below in the section “Combining multiple antennas”.

That was another key factor for Nokia’s initial proposal to modify the UE model in 3GPP to obtain more realistic antenna placements, thus frequency-dependent antenna combining.

Rel-19 3GPP UE antenna polarization

The reference UE radiation pattern for a handheld device (as described in Table 14 and depicted in Figure 17) is positioned and aligned within the UE local coordinate system (LCS → x', y', z'). As illustrated in Figure 19, the maximum gain direction is oriented perpendicular to the face (front) of the UE, with the positive Z-axis in this example.

Figure 19. Reference orientation of the reference radiation pattern for a handheld device

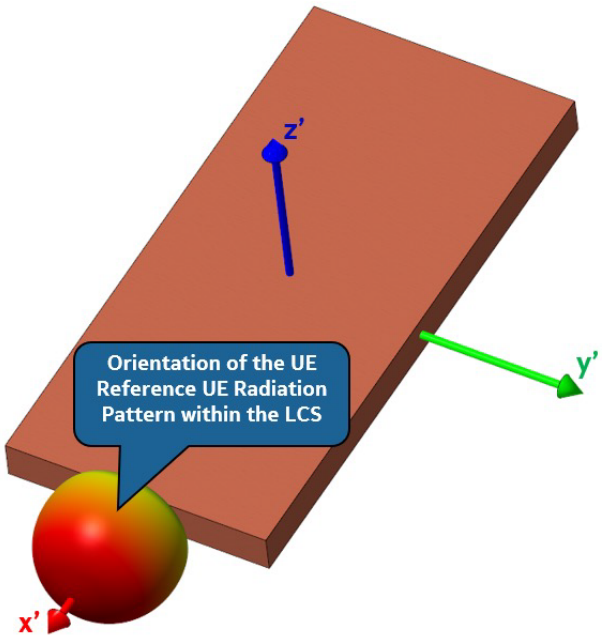

This gain rotation from the ACS to the LCS can be performed by using the 3D rotation equations 7.1.7 and 7.1.8 defined in 38.901 [3] and shown below.

$$\theta'(\alpha,\beta,\gamma;\theta'',\phi'') = \operatorname{acos}\left(\cos\beta\cos\gamma\cos\theta'' + (\sin\beta\cos\gamma\cos(\phi''-\alpha) - \sin\gamma\sin(\phi''-\alpha))\sin\theta''\right)$$

$$\phi'(\alpha,\beta,\gamma;\theta'',\phi'') = \arg\begin{pmatrix}(\cos\beta\sin\theta\cos(\phi-\alpha) - \sin\beta\cos\theta) + \\ j(\cos\beta\sin\gamma\cos\theta + (\sin\beta\sin\gamma\cos(\phi-\alpha) + \cos\gamma\sin(\phi-\alpha))\sin\theta)\end{pmatrix}$$

The reference UE radiation gain pattern positioned at the reference location in the LCS is then rotated to one of the eight potential antenna locations, as illustrated in Figure 20 for the antennas located at the four corners of the handheld form factor (Ant#1, Ant#3, Ant#5 and Ant#7).

Figure 20. Rotations of the UE reference antenna gain pattern to the four locations at the corners of the handheld device, where the yellow arrows indicate the α rotations and the green arrows the γ rotations

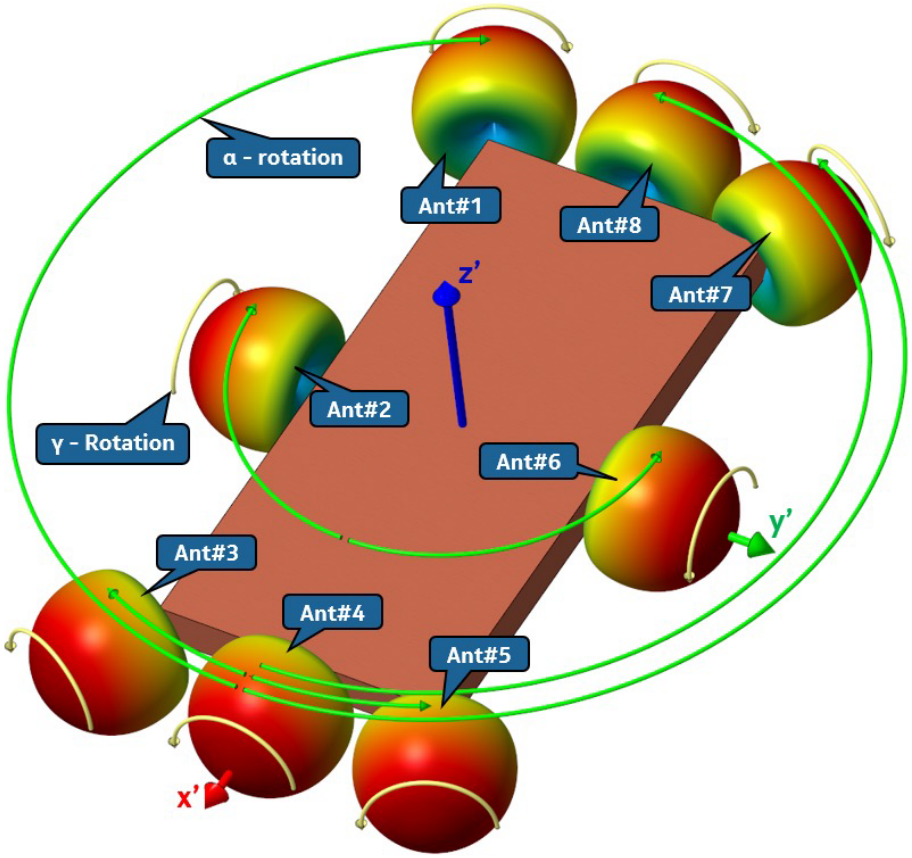

The reference UE radiation pattern, being a gain pattern, does not inherently contain specific θ and ϕ field components. Instead, it has all power in only one of the field components, depending on the chosen definition. However, both of the θ and ϕ field components can be derived by applying the rotation matrix defined in 38.901 equation 7.1-11 [3] to rotate the reference UE radiation pattern from its reference orientation and position (as illustrated in Figure 19) with all its power in the θ field component: $F\_\theta\,(\theta'',\phi'') = \sqrt{(A(\theta'',\phi''))}$ and $F\_\phi\,(\theta'',\phi'') = 0$, to one of the potential UE antenna locations shown in Figure 18.

$$\begin{pmatrix} F_{\theta'}(\theta',\phi') \\ F_{\phi'}(\theta',\phi') \end{pmatrix} = \begin{pmatrix} +\cos(\psi) & -\sin(\psi) \\ +\sin(\psi) & +\cos(\psi) \end{pmatrix} \begin{pmatrix} F_{\theta''}(\theta'',\phi'') \\ F_{\phi''}(\theta'',\phi'') \end{pmatrix}$$

Where cos(ψ) and sin(ψ) are defined as follows:

$$\cos\psi = \frac{\cos\beta\cos\gamma\sin\theta'' - (\sin\beta\cos\gamma\cos(\phi''-\alpha) - \sin\gamma\sin(\phi''-\alpha))\cos\theta''}{\sqrt{1-(\cos\beta\cos\gamma\cos\theta'' + (\sin\beta\cos\gamma\cos(\phi''-\alpha) - \sin\gamma\sin(\phi''-\alpha))\sin\theta'')^2}}$$

$$\sin\psi = \frac{\sin\beta\cos\gamma\sin(\phi''-\alpha) + \sin\gamma\cos(\phi''-\alpha)}{\sqrt{1-(\cos\beta\cos\gamma\cos\theta'' + (\sin\beta\cos\gamma\cos(\phi''-\alpha) - \sin\gamma\sin(\phi''-\alpha))\sin\theta'')^2}}$$

The rotation of the reference UE radiation pattern, having all its power in the theta field component ($F_{\theta''}(\theta'',\phi'')$), is perform in two steps ACS → LCS and LCS → GCS to obtain both polarized field components [$F_{\theta''}(\theta'',\phi'')$, $F\phi\,''(\theta'',\phi'')$]. The first rotation (ACS → LCS) is defined as shown in Table 15:

Table 15. Rotation values for the first rotation (ASC > LCS)

	Ant#1	Ant#2	Ant#3	Ant#4	Ant#5	Ant#6	Ant#7	Ant#8
α	90°	90°	90°	90°	90°	90°	90°	90°
β	0°	0°	0°	0°	0°	0°	0°	0°
γ	-155°	-90°	-25°	0°	25°	90°	155°	180°

The second rotation values from the LCS to the global coordinate system (GCS) are dependent on the use case for the phone (orientation), like one-hand browse, dual-hand browse, talk mode or free space (see Figure 7) and are defined as shown in Table 16.

Table 16. Rotation values for the second rotation (LSC > GCS)

	One-hand browse	Dual-hand browse	Head and hand	Free space
α	0° - 360°	0° - 360°	0° - 360°	0° - 360°
β	45°	0°	90°	45°
γ	0°	45°	0°	0°

The total gain and the θ and ϕ field components are shown in Figure 21 for Ant#1, Ant#3, Ant#5 and Ant#7 for a UE oriented in either free space or one-hand browse.

Figure 21. θ and ϕ polarization components as a result of the rotation of the individual UE reference antenna gain patterns with the device in free space or one-hand browse orientation

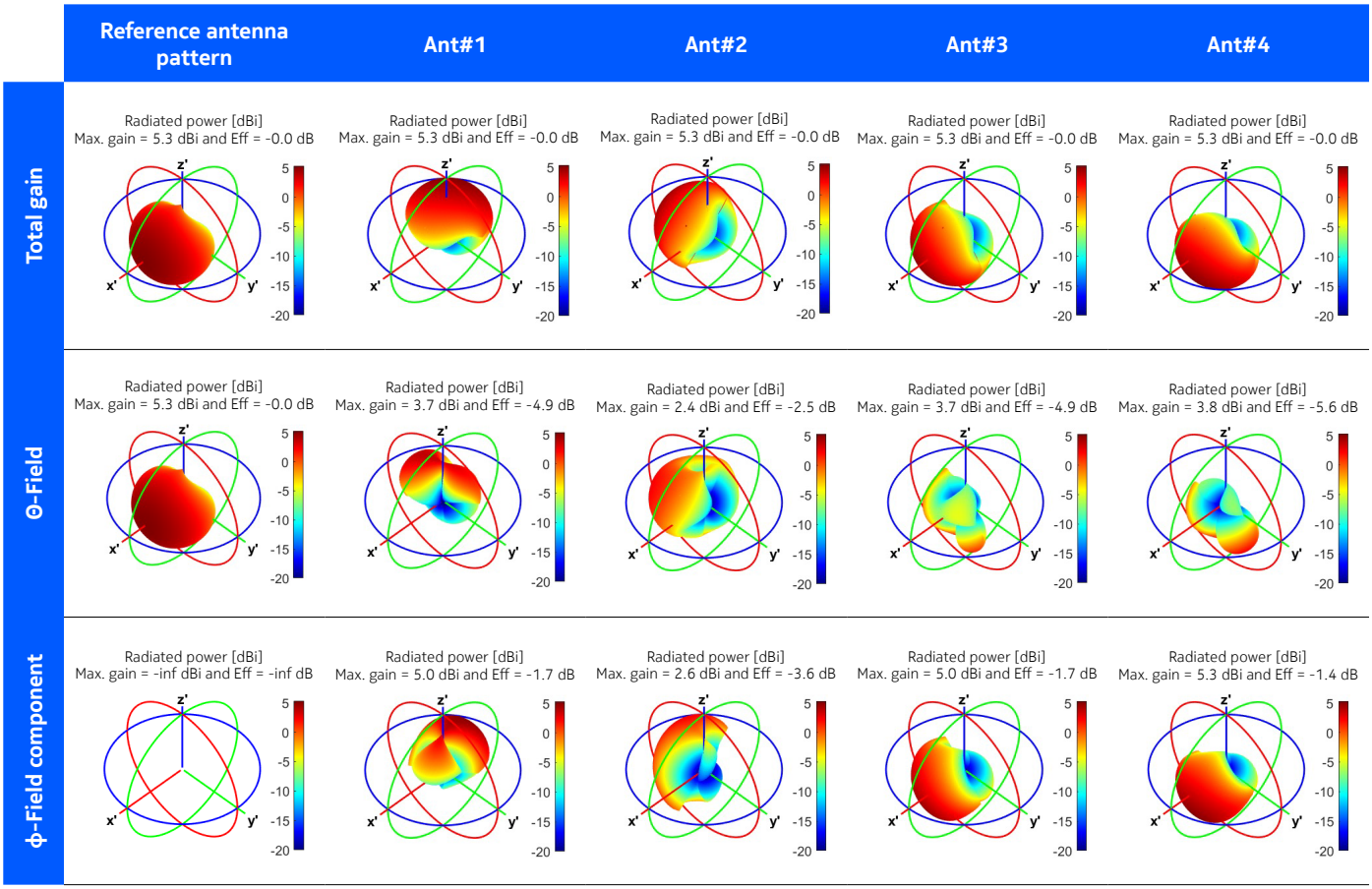

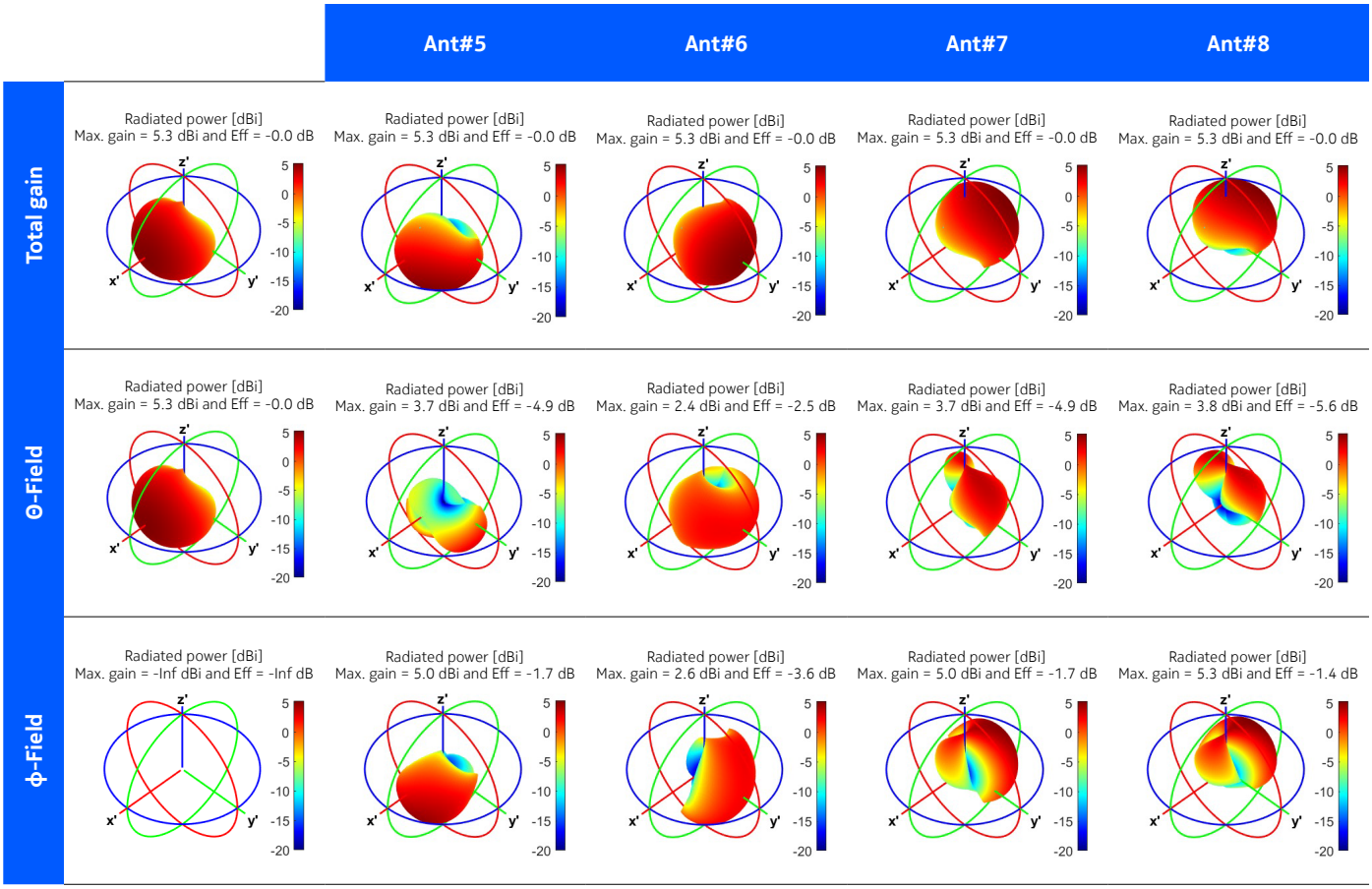

The total gain and the θ and ϕ field components for a UE oriented in dual-hand browse are shown in Figure 22 for all eight antennas at the defined locations on the reference UE form-factor.

Figure 22. θ and ϕ polarization components as a result of the rotation of the individual UE reference antenna gain patterns with the device in dual-hand browse orientation: a) total gain b) Theta field component c) Phi field component

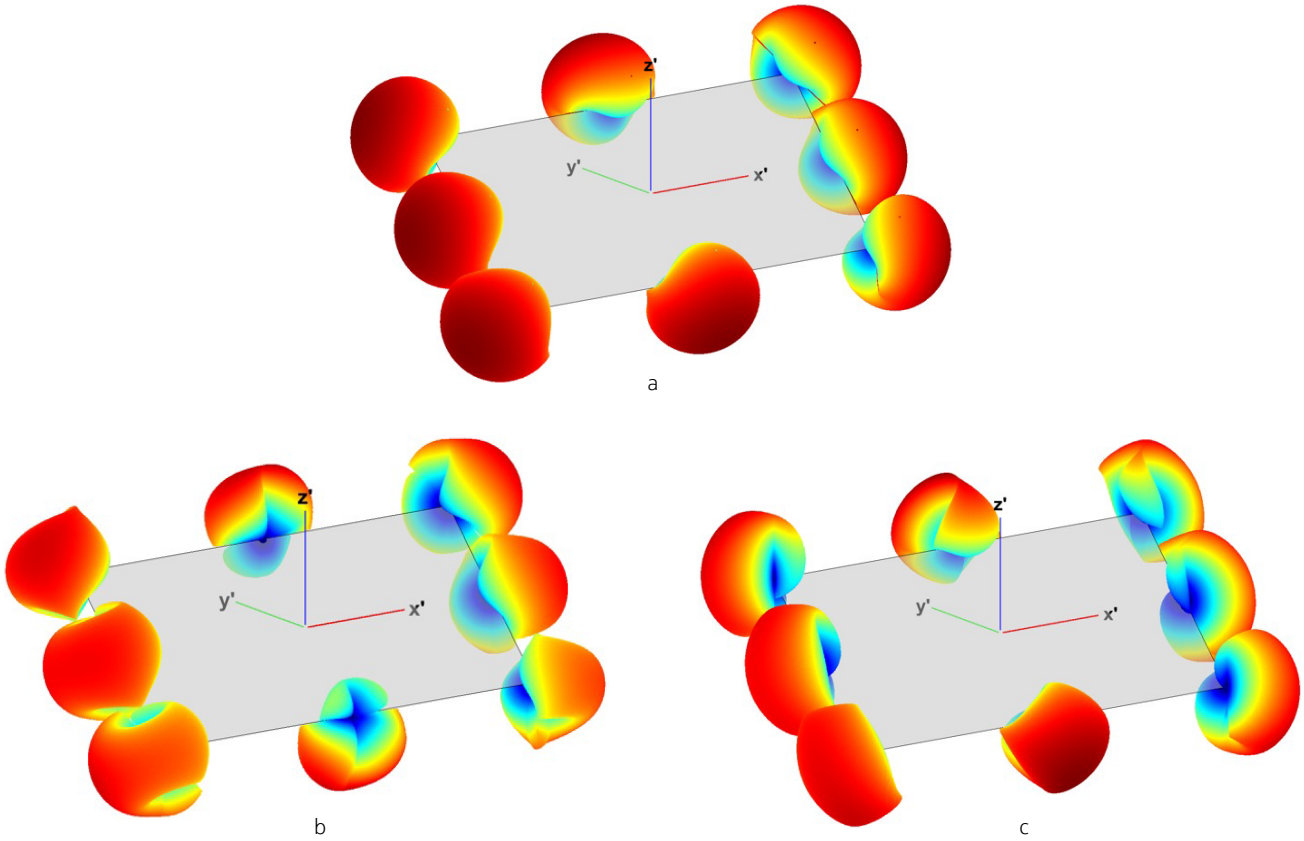

The derived reference θ and ϕ polarization components are good approximations for θ and ϕ polarization components observed for antennas implemented on smartphones, as illustrated in Figure 12. This improved representation of the complex antenna characteristics was a crucial aspect of Nokia's initial proposal to modify the UE model in 3GPP, enabling the introduction of specific θ and ϕ polarization components for each antenna, depending on its physical location on the device.

Rel-19 3GPP single antenna compared with Nokia 6G reference smartphone

The development of the new UE antenna reference radiation pattern for handheld devices aimed to strike a balance between simplicity and accuracy. Two primary objectives guided this effort:

1. **Reuse of existing 3GPP equations**

   The new reference radiation pattern was designed to leverage the equations already included in the 3GPP specification (Table 7.3-1, TS 38.901) with a new set of parameters (Table 14). This approach facilitated a more straightforward implementation while maintaining consistency with existing standards.

2. **Frequency independent reference radiation pattern**

   The second objective was to utilize the same reference radiation pattern across all frequencies. This decision was made to prioritize simplicity, acknowledging that it might result in some discrepancies compared to frequency-dependent radiation patterns, such as those simulated for the Nokia 6G reference smartphone. Keep in mind that the combing of the frequency independent reference radiation patterns will result in frequency dependent UE total radiation patterns due to the fixed physical distance between the antenna locations (Figure 18).

   Although this approach led to some compromises, the agreed 3GPP Rel-19 reference radiation pattern demonstrates an acceptable approximation compared to the simulated radiation patterns of the Nokia reference UE. This is illustrated in Figure 22, as 2D-Cut where the z-axis of the used coordinate system has been aligned the maximum gain direction of the individual simulated and normalized radiation patterns of the Nokia 6G reference phone, and for the new 3GPP UE reference antenna pattern.

Figure 23. 2D radiation cuts and CCDF plot of the directivity of the antennas of the Nokia 6G reference smartphone and the single antenna 3GPP Rel-19 reference antenna: a) top view b) side view c) front view d) CCDF curve of the coverage

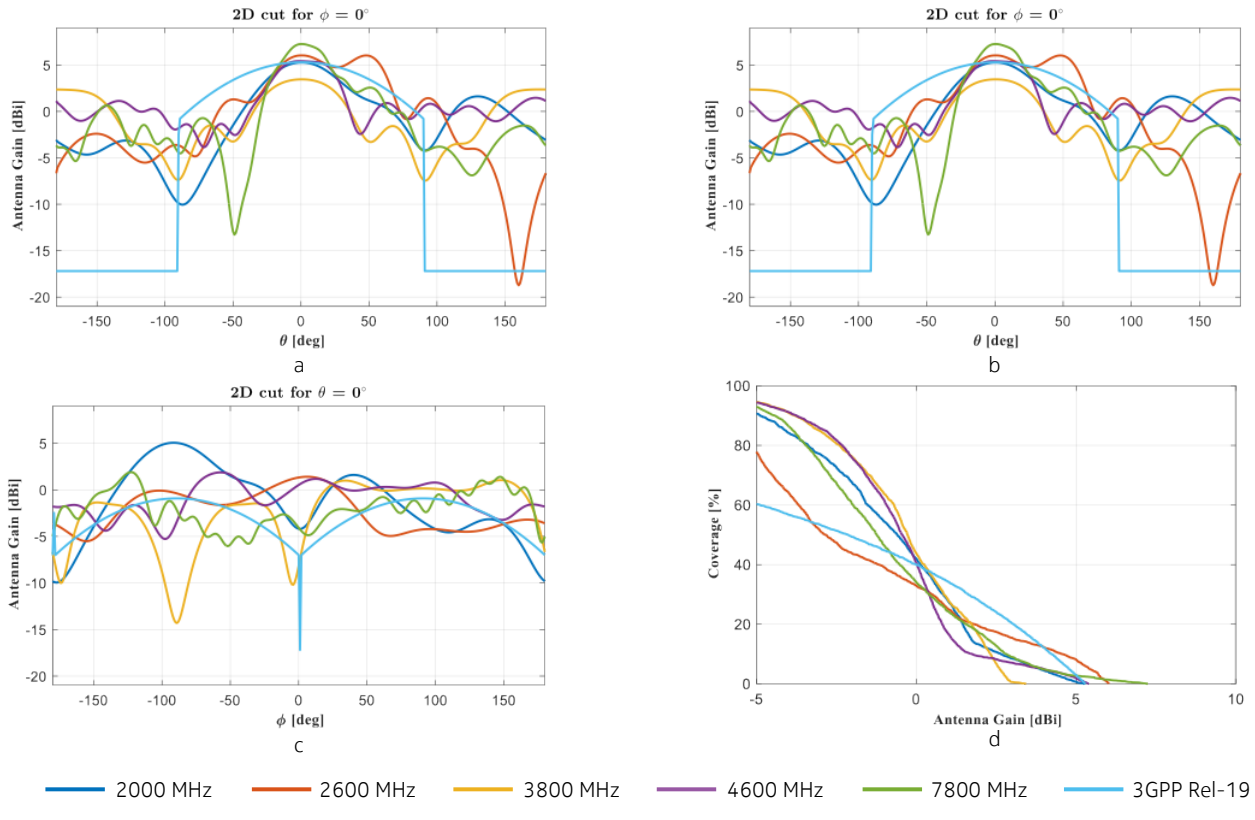

The approximation of the reference radiation pattern is more accurate in regions of high antenna gain, as evident from Figure 23. This is particularly relevant for handheld devices, such as smartphones, which typically employ multiple antennas. In these devices, individual antennas are predominantly utilized in angular directions corresponding to their peak gains, thereby minimizing the impact of discrepancies in the low gain regions.

Combining of multiple antennas

Antenna combining, assuming a ULA, yields predictable radiation patterns with a well-defined main beam and suppressed side lobes, as depicted in Figure 3. Conversely, antennas with realistic UE form factors exhibit non-uniform radiation patterns, where the power is mixed between both polarization components (θ and ϕ). This is because the antennas are implemented as single feed structures. In addition, the non-uniform fixed physical antenna element spacings will often deviate from the ideal half-wavelength separation depending on the configured system frequency.

As the radiation patterns obtained for EM simulations of the Nokia 6G reference smartphone are complex numbers including phase information, they can be combined using superposition. However, as the new UE antenna reference radiation pattern is a gain-only pattern (no phase information), individual antennas are combined using the array factor (AF) taking the physical distance between the antennas into account.

Nokia 6G reference smartphone

Combining the antennas of the Nokia reference 6G phone is based on superposition of the individual complex radiation patterns using the formula below.

$$ComRP(\theta,\phi) = \sum_{x=1}^{n} a_n(\theta,\phi) + i * (b_n(\theta,\phi) + \psi)$$

Where a is the real and b the imaginary gain values, n is the number of combined APs, θ and ϕ are the spherical coordinates and ψ is the precoding value for that specific AP.

Some of the combing radiation patterns are shown in Figure 24 at different frequencies, for different numbers of combined APs, and with a 0° phase offset (ψ) between the combined APs.

Figure 24. Superposition of radiation patterns obtained in free space with the Nokia 6G reference smartphone

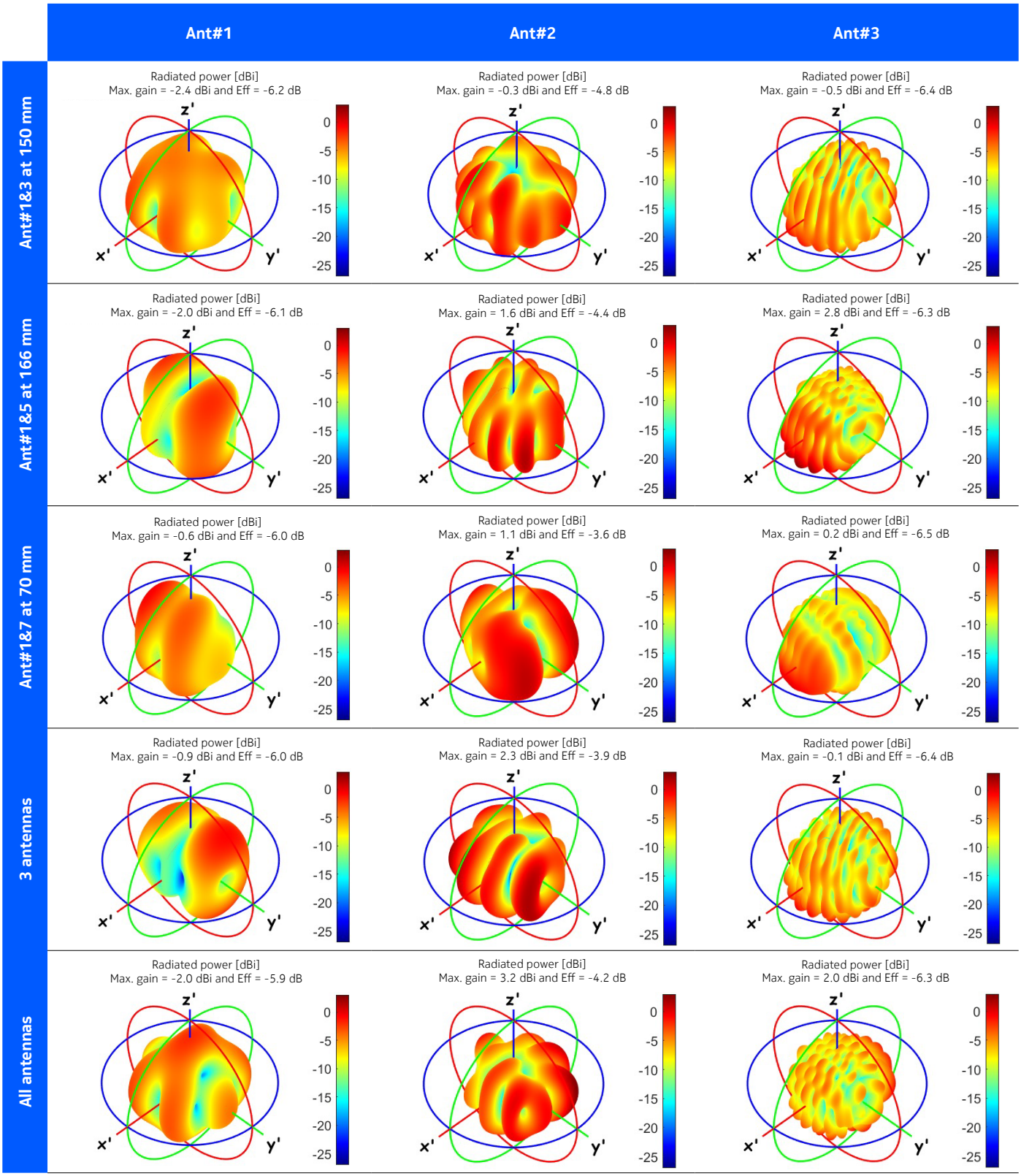

The combined radiation patterns of handheld device antennas deviate significantly from those obtained under the ULA assumption. As illustrated in Figure 24, the combined radiation patterns exhibit more ripples and are less predictable, particularly at higher frequencies (2000–7800 MHz), since the electrical length of the fixed physical distances between the antennas increases with frequency.

In contrast to the expected 3 dB increase in antenna gain for every doubling of the number of combined antennas in a ULA, handheld devices often experience a reduced gain increase when combining multiple antennas. This is due to differences in antenna gain and relative phase values between antennas for a given angular direction.

1. **Power**

   Even with ideal antenna combining, the maximum antenna gain is not increased by 3 dB for two antennas as the maximum power of each antenna element is in different angular directions. A 3 dB increase in antenna gain is only achievable in angular directions where both radiation patterns have the same gain values, assuming ideal phase conditions. However, the absolute gain values at those angular directions will be lower than the maximum antenna gain values of the individual antenna element.

2. **Phase**

   The relative phase differences for the θ and ϕ field-components can be significantly different (e.g., 56° and 217°, respectively) for a given angular direction. Since each antenna has only one feed port, only one pre-coding phase value can be applied, preventing optimal antenna power combining for most angular directions. As a result, optimal power combining is seldom possible for antennas on handheld devices.

While pre-coding/antenna combining can increase the maximum antenna gain, it does not achieve the expected 6 dB increase from four antennas, as shown in Table 17. In fact, some pre-coding values may result in reduced maximum antenna gain compared to the maximum gain for a single antenna element. For example, four antennas combined for 2000 MHz with 0° phase differences will result in a maximum combined antenna gain of -2.3 dBi (see Figure 24, lower left example), where the maximum gain of a single antenna is -1.3 dBi.

Table 17. Gains in maximum antenna gain and efficiency when utilizing superposition for precoding with a full 90° codebook with the Nokia 6G reference smartphone

	Maximum gain			Efficiency		
	Antenna selection	**Full codebook**	**Delta**	**Antenna selection**	**Full codebook**	**Delta**
2000 MHz	-1.3 dBi	-0.4 dBi	0.9 dB	-4.8 dB	-2.5 dB	2.3 dB
2600 MHz	-0.4 dBi	1.9 dBi	2.3 dB	-3.5 dB	-2.1 dB	1.4 dB
3800 MHz	-0.6 dBi	3.2 dBi	3.8 dB	-2.6 dB	0.3 dB	2.9 dB
4600 MHz	-1.3 dBi	1.1 dBi	2.4 dB	-5.1 dB	-2.5 dB	2.6 dB
7800 MHz	0.8 dBi	2.8 dBi	2.0 dB	-4.3 dB	-2.3 dB	2.0 dB
Average	**-0.5 dBi**	**1.9 dBi**	**2.4 dB**	**-4.0 dB**	**-1.7 dB**	**2.3 dB**

The Nokia 6G reference phone exhibits an increase in maximum combined antenna gain, ranging from 0.9–3.8 dB, with an average frequency-dependent increase of 2.4 dB. The highest increases are predominantly observed at frequencies where individual radiation patterns exhibit lower directivity.

To illustrate this phenomenon, consider the directivity of the individual antennas at 3800 MHz, which is 3.5 dBi. Consequently, the combined maximum gain increases by 3.8 dB. In contrast, at 7800 MHz, the directivity of the individual antennas is significantly higher at 7.3 dBi but only results in a relatively lower increase with a combined maximum gain of 2.0 dB.

The underlying reason for this behavior is the increased likelihood of multiple radiation patterns with high gain in the same angular direction for patterns with lower directivity. Furthermore, the angular directions of the maximum antenna gain of the individual antennas play a crucial role in determining the obtained combining gain. Specifically, overlapping high gain regions in the angular domain result in increased antenna combining gains.

These findings highlight the importance of considering the directivity and angular characteristics of individual radiation patterns when optimizing antenna combining gain in handheld devices like smartphone.

The utilization of a full codebook with a 90° phase granularity (156 possible precoding values) yields improved power envelope efficiency, as evident in Table 17, with observed gains of 2–3 dB across the simulated frequencies, relative to selecting the optimal antenna individually for each angular direction. This performance enhancement is further visualized through CCDF curves of the power envelope, as depicted in Figure 25. The blue curve represents antenna switching/selection, whereas the red curve illustrates the power envelope efficiency achieved by leveraging the full codebook.

Figure 25: Coverage (CCDF) for BAS and antenna precoding using a full 90° codebook with the Nokia 6G reference smartphone at: a) 2000 MHz b) 3800 MHz c) 7800 MHz

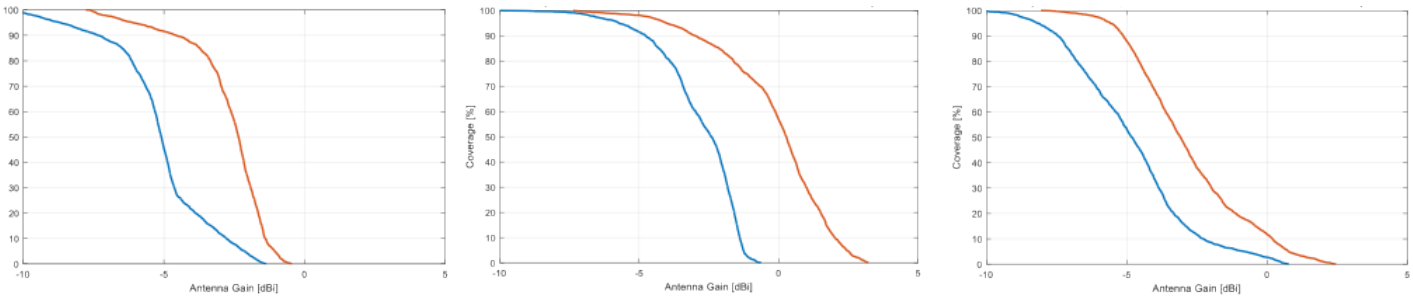

a b c

The distribution of the number of combined APs that result in the maximum antenna gain for a given angular direction are shown in Table 18.

Table 18. Distribution of the number of combined APs that result in the maximum antenna gain for a given angular direction for the Nokia 6G reference smartphone

	Number of combined APs for max coverage			
	1 AP	2APs	3 APs	4 APs
2000 MHz	0.0 %	11.6 %	17.1 %	71.3%
2600 MHz	4.4 %	36.2 %	28.3 %	31.1%
3800 MHz	0.0 %	2.4 %	47.8 %	50.0 %
4600 MHz	0.0 %	11.9 %	25.8 %	62.3 %
7800 MHz	1.2 %	20.0 %	28.7 %	50.1 %
Average	**1.1 %**	**16.4 %**	**29.5 %**	**53.0 %**

The results in Table 18 show that maximum precoding antenna gains are only obtained using all four AP for approximately 50% of the angular domain, which is half of what is achieved with a uniform linear antenna array, as assumed with the old 3GPP UE antenna model.

New 3GPP UE antenna model

Combining the antennas of the new 3GPP UE antenna model cannot be done by using superposition, as the reference radiation pattern is an absolute gain pattern without a phase component. Instead, the combining is based on the AF derived between each set of APs to be combined, taking into account the physical distances between the APs, the system frequency, and the pre-coding vector. The formula used for the AF is shown below.

$$ComRP(\theta,\phi) = \sqrt{\frac{1}{n}\sum_{x=1}^{n} UE_{AP(n)}(\theta,\phi)\cdot e^{i\left(\frac{2\pi}{\lambda}\left(x_{dim}(n)(\sin(\theta)\cos(\phi)+y_{dim}(n)(\sin(\theta)\sin(\phi))+\psi\right)\right)}}$$

Where n is the number of combined APs, $UE_{AP(n)}$ is the radiation pattern of n's AP, θ and ϕ are the spherical coordinates, x_{dim} and y_{dim} are the physical distances between two APs, and ψ is the precoding value for that specific AP.

Some of the derived AF 3D patterns are shown in Figure 26 at different frequencies, with varying numbers of combined antennas, all with a 0° phase offset (ψ) and equal amplitude between the combined APs.

Figure 26. Examples of the AFs used for combining antenna radiation gain patterns with the new 3GPP UA antenna model

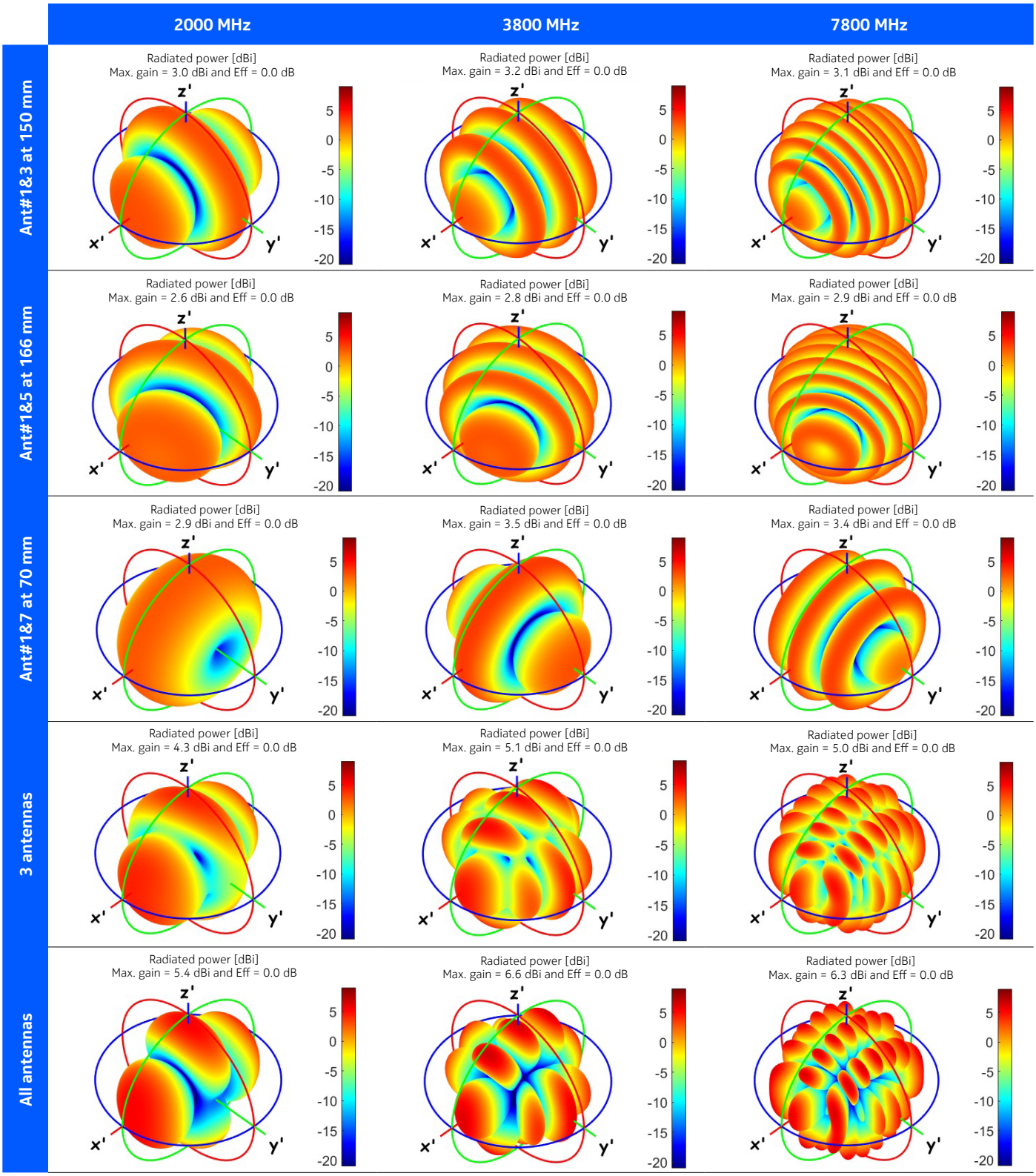

The combined radiation patterns using the new 3GPP UE antenna model are shown in Figure 27 for different frequencies using the AFs shown in Figure 26.

Figure 27. Examples of the AFs used for combining antenna radiation gain patterns with the new 3GPP UA antenna model

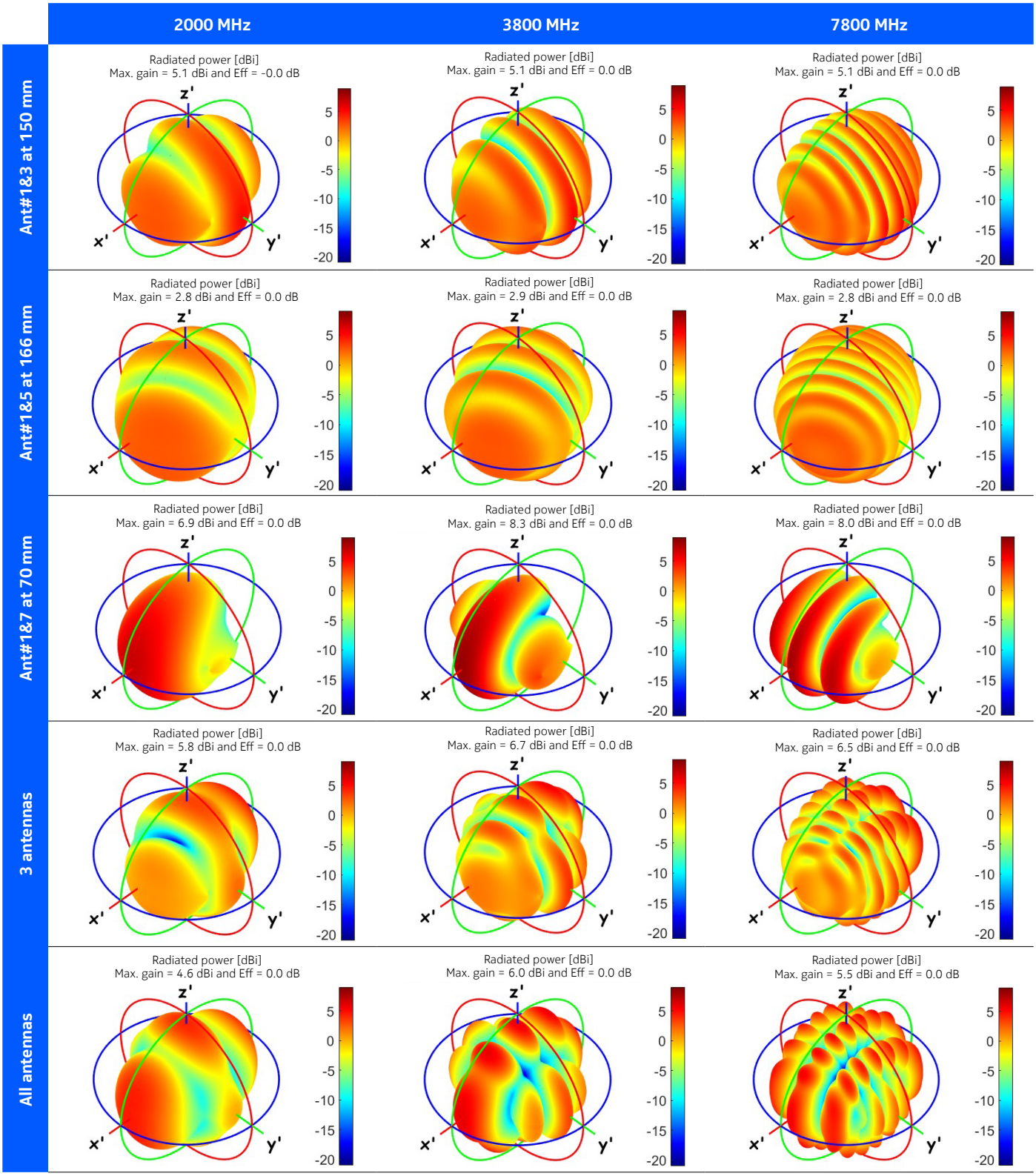

The results in Figure 27 demonstrate that the obtained radiation patterns are significantly affected by the AF, showing the same ripple behavior as the example radiation patterns obtained from the Nokia 6G reference smartphone. While the overall goal is not to replicate identical radiation patterns as obtained from the Nokia 6G reference smartphone, the objective is to develop a 3GPP UE antenna model that captures similar antenna characteristics, like the overall shape, the ripple, maximum gain values, and angular directions with nulls (low combined antenna gain compared to uniform antennas).

This is essential for ensuring that the model accurately represents the behavior of real-world devices and the performance gains achieved using the new UE antenna model and pre-coding/antenna combining. The results are summarized in Table 19.

Table 19. Gains in maximum antenna gain and efficiency when utilizing the array factor for precoding with a full 90° codebook with the new 3GPP UA antenna model

	Maximum gain			Efficiency		
	Antenna selection	**Full codebook**	**Delta**	**Antenna selection**	**Full codebook**	**Delta**
2000 MHz	5.3 dBi	7.3 dBi	2.0 dB	3.6 dB	5.4 dB	1.8 dB
2600 MHz	5.3 dBi	7.7 dBi	2.4 dB	3.6 dB	5.5 dB	1.9 dB
3800 MHz	5.3 dBi	8.3 dBi	3.0 dB	3.6 dB	5.5 dB	1.9 dB
4600 MHz	5.3 dBi	8.0 dBi	2.7 dB	3.6 dB	5.4 dB	1.8 dB
7800 MHz	5.3 dBi	8.0 dBi	2.7 dB	3.6 dB	5.5 dB	1.9 dB
Average	**5.3 dBi**	**7.9 dBi**	**2.6 dB**	**3.6 dB**	**5.5 dB**	**1.9 dB**

The average delta values in Table 19 demonstrate a comparable performance to those obtained from the Nokia 6G reference smartphone (2.4 and 2.3 dB, see Table 17), albeit with reduced frequency variation. This is a consequence of the design choice for the new 3GPP UE antenna model, which employs a single reference radiation pattern across all frequencies for simplicity.

The discrepancies of the combined radiation patterns between the Nokia 6G reference smartphone and the new 3GPP UE antenna model stem from the differing methods used for combining. The simulated radiation patterns for the Nokia 6G reference smartphone incorporate complex numbers with phase information, which are combined using the superposition principle. In contrast, the new 3GPP UE antenna model relies on the AF for combining, using an absolute gain pattern without phase information.

A key distinction between the old and new 3GPP UE antenna models lies in the electrical length between the combined radiation patterns, which introduces frequency-dependent behavior in the combined radiation patterns. This characteristic is reflected in the CCDF curves of the power envelope, as shown in Figure 28 for antenna switching/selection (blue curve) and utilizing the full codebook (red curve).

Figure 28. Coverage (CCDF) for BAS and antenna precoding using a full 90° codebook with the new 3GPP UA antenna model at: a) 2000 MHz b) 3800 MHz c) 7800 MHz

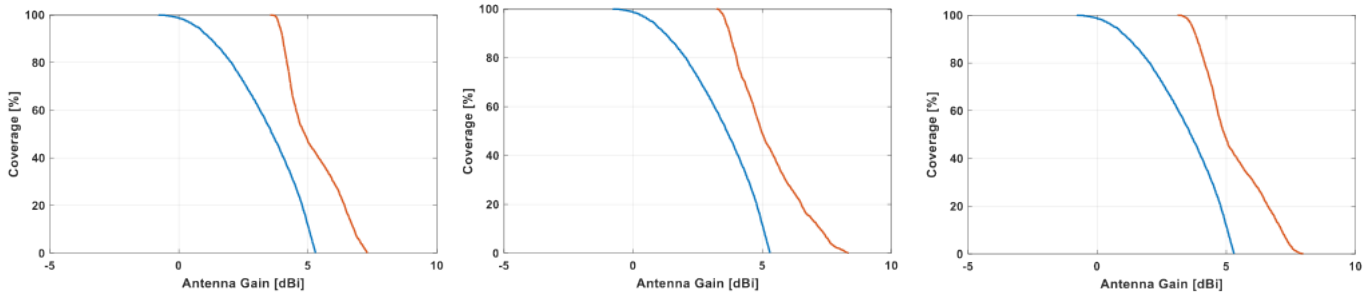

The distribution of the number of combined APs that result in the maximum antenna gain for a given angular direction are shown in Table 20 for the new 3GPP UE antenna model, which also shows limited variation over frequency.

Table 20. Distribution of the number of combined APs that result in the maximum antenna gain for a given angular direction for the new 3GPP UE antenna model

	Number of combined APs for max coverage			
	1 AP	**2APs**	**3 APs**	**4 APs**
2000 MHz	0.3 %	62.2 %	14.0 %	23.5 %
2600 MHz	1.0 %	67.0 %	11.9 %	20.1 %
3800 MHz	2.3 %	66.6 %	14.6 %	16.5 %
4600 MHz	3.4 %	67.5 %	10.0 %	19.2 %
7800 MHz	3.5 %	67.2 %	10.6 %	18.8 %
Average	**2.1 %**	**66.1 %**	**12.2 %**	**19.6 %**

The average distribution values of the number of used APs for maximum coverage are not exactly the same as those obtained for the Nokia 6G reference smartphone but do show a similar trend with one dominant AP configuration for both cases. Specifically, the new UE antenna model tends to favor a configuration of two APs, whereas the Nokia 6G reference smartphone exhibits a preference for four APs. Keep in mind that the old 3GPP UE antenna model consistently achieves maximum gain values using four APs across the entire angular domain, a behavior that is not representative of real-life devices.

Rel-15 model: a self-blockage definition

The stochastic blockage model A for self-blocking is define in TR 38.901 [3], section 7.6.4.1, where a self-blocking region is defined in terms of an angular direction (θ'_{sb},Φ'_{sb}) with an angular span of (x_{sb},y_{sb}), expressed as follows.

$$\left\{\theta', \phi' \middle| \left(\theta'_{sb} - \frac{y_{sb}}{2} \leq \theta' \leq \theta'_{sb} + \frac{y_{sb}}{2}, \phi'_{sb} - \frac{x_{sb}}{2} \leq \phi' \leq \phi'_{sb} + \frac{x_{sb}}{2}\right)\right\}$$

The values of Φ'_{sb}, x_k, Φ'_{sb} and x_k are given in Table 21.

Table 21. Self-blocking region parameters (Table 7.6.4.1-1 from TS 38.901)

	Φ'_{sb}	x_k	θ'_{sb}	y_{sb}
Portrait mode	260°	120°	100°	80°
Landscape mode	40°	160°	110°	75°

The attenuation factor used for antenna gain values within the specified blockage region is 30 dB. This approach leads to a uniform angular attenuation across the region, which is consistent for all implemented antennas on the device. This is illustrated in Table 22, which includes free-space, 3D stereographic projection plots of the Nokia reference smartphone at 2600 MHz as reference (see previous section “Radiation patterns for free space”), as well as free-space plots with an overlay illustrating the current 3GPP portrait self-blocking region and plots obtained including the CTIA right-hand browsing phantom (see previous section “Radiation patterns for CTIA right-hand browsing”).

Figure 29. The stochastic blockage model A for self-blocking used by 3GPP Rel-15

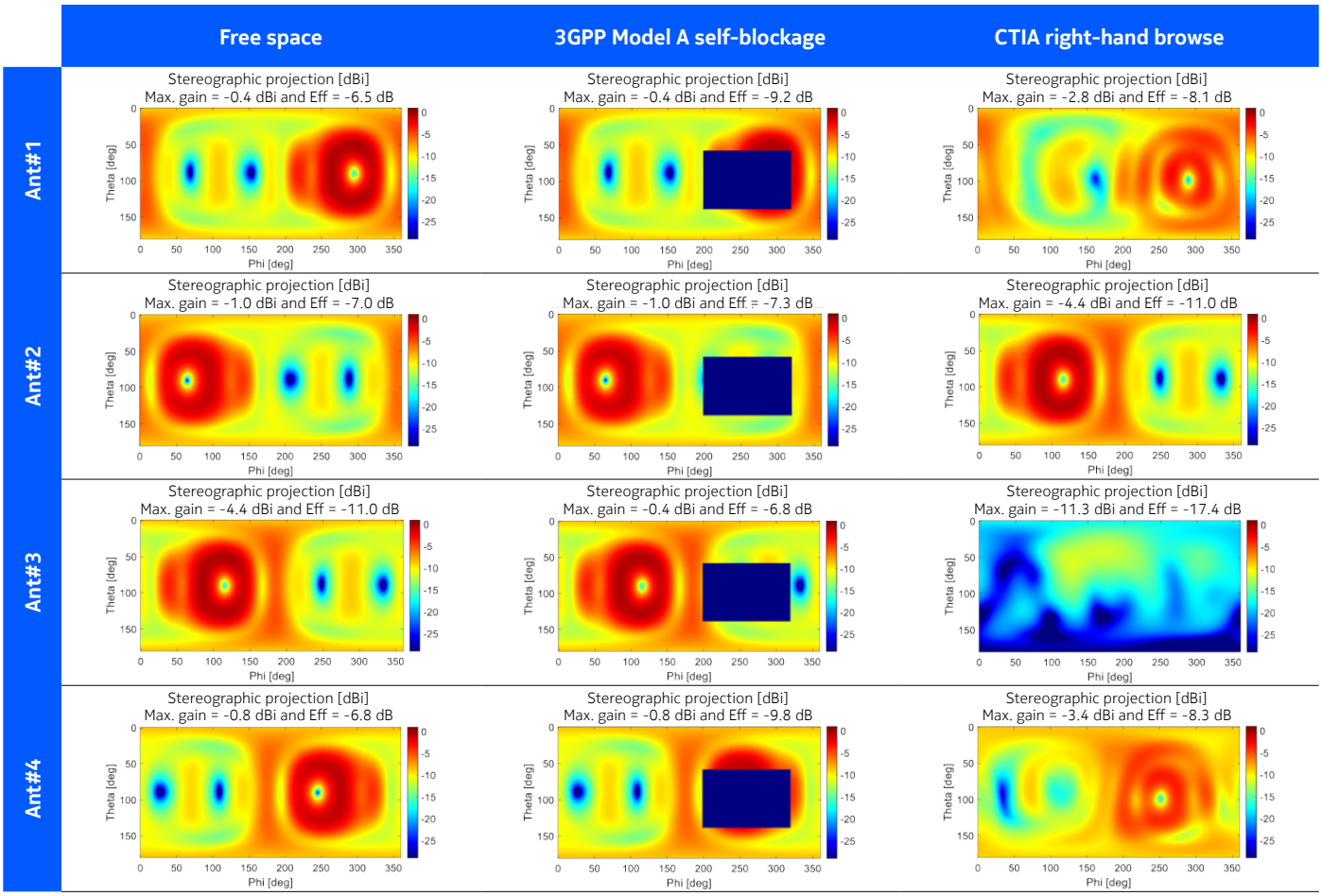

The current 3GPP blockage model A for self-blocking at a UE exhibits unrealistic behavior, particularly with regards to maximum gain and antenna efficiency. As shown in Table 22, the maximum gain values of all the antennas remain unchanged, while there is a noticeable effect on antenna efficiency, with a reduction of 0.3 to 3.0 dB. Nevertheless, the observed reductions to the maximum antenna gain and efficiency are too small for the affected antennas when compared to the results obtained with the Nokia 6G reference smartphone—including the CTIA right-hand browse phantom. Specifically, the observed reductions in maximum antenna gain and efficiency using the current blockage model A for self-blocking are more than 10 dB lower than expected for some antennas.

Rel-19 3GPP spatial non-stationarity at UE side

The new spatial non-stationarity (SNS) model fundamentally deviates from the legacy approach of employing a uniform blockage region in a specific angular domain for all implemented antennas. Instead, this new near-field blockage model utilizes distinct attenuation factors tailored to the specific locations of each antenna. These attenuation values are derived from simulations conducted with the hand/head phantoms, providing a more accurate representation of the blockage effects on individual antennas for different use cases. This approach is exemplified in Table 23 for a one-hand browse use case, including simulation results at 2600 MHz in free space and with the CTIA right-hand browse phantom.

Figure 30. 3GPP Rel-19 near-field blockage model illustrated for CTIA right-hand browse

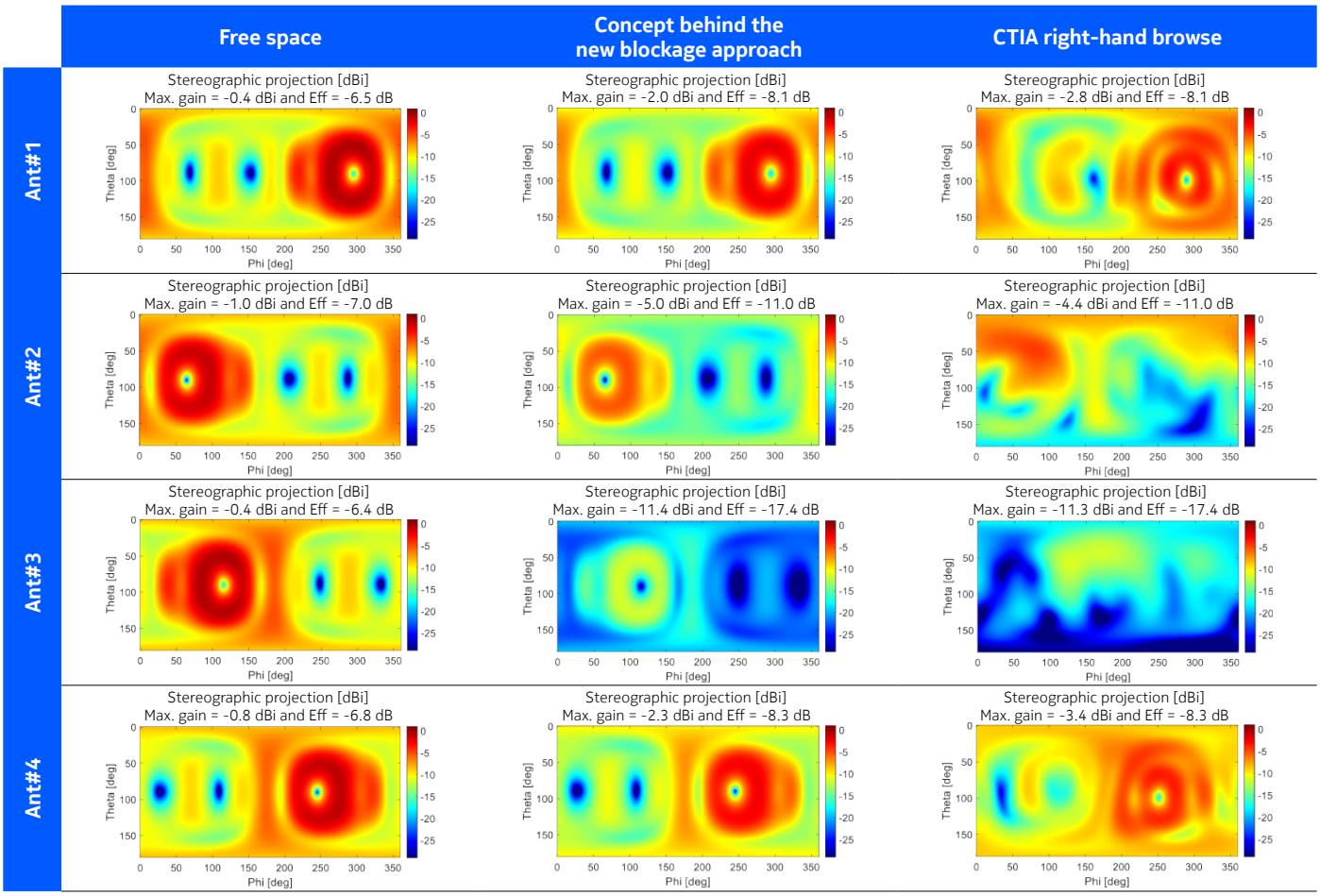

It is clear that the proposed new near-field blockage model offers a more accurate representation of the changes in antenna characteristics that occur when a user is holding a handheld device. The key distinction between the existing 3GPP stochastic blockage model A for self-blocking and the new approach lies in the use of location-specific attenuation values for different antennas on the device form factor, which are derived from simulations incorporating hand phantoms. This approach also provides a more realistic representation of the AP power imbalance caused by the user's presence. This result was a key driver of Nokia's initial proposal to modify the UE model within 3GPP.

While the existing stochastic blockage model A can still be utilized to represent user body blockage, it may be necessary to define a new angular region to achieve accurate results for this specific use case.

User contribution to near-field blockage

The final values used for the near-field attenuations are based on simulation results. Specifically, for frequencies below 1.0 GHz, and for the frequency range 1.0–8.4 GHz (averaged across 2000, 2600, 3800, 4600, and 7800 MHz), the employed attenuation values are based on simulation results obtained using the Nokia reference 6G smartphone. These results can be found above in the sections "Antenna efficiencies for CTIA right-hand browsing", "Efficiencies for Nokia dual-hand browsing", and "Efficiencies for CTIA head and hand right side".

Table 24. 3GPP near-field blockage attenuation values for each defined antenna location

Antenna index	Near-field power attenuation [dB]					
	One-hand grip		Dual-hand grip		Head and one-hand grip	
	Below 1 GHz	1–8.4 GHz	Below 1 GHz	1–8.4 GHz	Below 1 GHz	1–8.4 GHz
1	-	0.7	-	11.0	-	3.7
2	-	4.1	-	1.1	-	4.6
3	-	3.3	-	10.5	-	4.3
4	13.6	7.2	5.8	5.6	15.1	7.8
5	-	10.8	-	1.5	-	11.7
6	-	9.1	-	1.4	-	10.1
7	-	0.7	-	1.3	-	2.9
8	2.4	0.6	5.6	6.2	4.9	4.2

The probability for each scenario (user grip) when doing SLS is defined in Table 25, where 90% of the UE will be affected by one of these three user scenarios.

Table 25. The probability of each scenario

Usage scenario	One-hand grip	Dual-hand grip	Head and one-hand grip
Probability	58%	29%	13%

Conclusion

The legacy 3GPP (Rel-15) UE antenna model assumes a uniform linear array (ULA) with a half-wavelength electrical distance between uniform linear elements. This approach is not suitable for handheld devices like smartphones, which exhibit non-uniform antenna characteristics and non-uniform electrical distances between antennas.

These discrepancies in UE antenna characteristics between the model used for 3GPP simulations and the behavior observed for real-life smartphones were a key motivation for Nokia to develop a new UE antenna model that could be adopted by the existing framework already specified within 3GPP.

A new 3GPP UE antenna model is adopted in Rel-19, which is designed to accurately capture the complex antenna behavior in handheld devices. It introduces a directive UE reference antenna radiation gain pattern, which is considerably more realistic than an isotropic radiation pattern. The new model also specifies eight different antenna candidate locations along the edge of a 150 mm x 70 mm reference handheld device form factor, with the maximum antenna gain direction oriented and aligned with the X-axis, Y-axis, or one of two reference diagonal axes with a 25° tilt to the Y-axis.

The key differences between the old and new 3GPP UE antenna models are:

1. **Reference antenna pattern:** the new model uses a directive UE reference antenna radiation gain pattern, while the old model uses an isotropic radiation pattern
2. **Antenna locations**: the new model specifies eight different antenna locations on a reference smartphone form factor, while the old model assumes a stand-alone ULA
3. **Electrical distances:** the new model takes into account the non-uniform electrical distances between antenna ports due to the fixed physical distances of the reference smartphone form factor, while the old model assumes a uniform half-wavelength electrical distance
4. **Polarization components:** the new model includes θ and ϕ field components that are derived from the reference radiation gain pattern, where the power distribution in the angular domain depends on the orientation of the reference smartphone form factor in the global coordinate system.

The new 3GPP UE antenna model is designed to provide a more accurate representation of the complex antenna behavior in handheld devices, which is essential for ensuring the performance and reliability of 6G devices. The model's ability to capture the complex antenna behavior in handheld devices will enable more accurate system- and link-level simulations with 3GPP and lead to better design and optimization of cellular 6G technologies.

Abbreviations

3GPP	3rd Generation Partnership Project
5G	Fifth-generation NR
ACS	Antenna coordinate system
AF	Array factor
AP	Antenna port
BAS	Best antenna selection
CCDF	Complementary cumulative distribution function
CPE	Customer premises equipment
CST	Computer simulation technology
CTIA	Cellular Telecommunications Industry Association
DHB	Dual-hand browse
DL	Downlink
EM	Electro magnetic
eUHB	Extended ultra-high band
FBG	Frequency band groups
FCC	Federal Communications Commission
FPC	Flexible printed circuit
FS	Free space
GCS	Global coordinate system
gNB	NR base station
HB	High band
IEEE	Institute of Electrical and Electronics Engineers
LB	Low band
LCS	Local coordinate system
LLS	Link-level simulations
LTE	Long-term evolution
MB	Mid band
MCAD	Mechanical computer-aided design
MHB	Mid/high band
MIMO	Multiple input, multiple output
MLB	Mid-low-band
mmWave	Millimetre wave
NR	New radio access
OTA	Over the air
PCO	Phase center offset
SLS	System-level simulations
SNS	Spatial non-stationarity
TR	Technical report
TS	Technical specifications
UE	User equipment
UHB	Ultra-high band
ULA	Uniform linear array

References

[1] CST Microwave Studio, Microwave Studio, 2025.05 ed., 2025.

[2] CTIA, version 3.9.5 ed., Vols. Table c-3, 2022, p. page 458.

[3] 3GPP, TS 38.901, v19.1.0 ed., 2025.

About Nokia

At Nokia, we create technology that helps the world act together.

As a B2B technology innovation leader, we are pioneering networks that sense, think and act by leveraging our work across mobile, fixed and cloud networks. In addition, we create value with intellectual property and long-term research, led by the award-winning Nokia Bell Labs.

With truly open architectures that seamlessly integrate into any ecosystem, our high-performance networks create new opportunities for monetization and scale. Service providers, enterprises and partners worldwide trust Nokia to deliver secure, reliable and sustainable networks today – and work with us to create the digital services and applications of the future.

Nokia OYJ
Karakaari 7
02610 Espoo
Finland
Tel. +358 (0) 10 44 88 000

Document code: CID215108 (November)